

AD 732024

D D C  
RECEIVED  
NOV 5 1971  
RECEIVED



15 SEPTEMBER 1971

**DIELECTRIC RELAXATION  
AND ROCK GEOPHYSICAL  
CHARACTERISTICS**

**Semiannual Report  
15 March Through 15 September**

Submitted to  
U.S. Bureau of Mines (ARPA)  
Contract No. HO210026

Reproduced by  
**NATIONAL TECHNICAL  
INFORMATION SERVICE**  
Springfield, Va. 22161

Honeywell Document 12288-IR1

Unclassified

Security Classification

3200.8 (Att 1 to Encl 1)

Mar 7, 66

DOCUMENT CONTROL DATA - R & D		
<i>(Security classification of title, body of abstract and indexes; annotation must be entered when the overall report is classified)</i>		
1. ORIGINATING ACTIVITY (Corporate author) Honeywell Inc., Systems and Research Center, Research Dept., 2345 Walnut St., St. Paul, Minnesota 55113		2a. REPORT SECURITY CLASSIFICATION Unclassified
		2b. GROUP - - -
3. REPORT TITLE Dielectric Relaxation and Rock Geophysical Characteristics		
4. DESCRIPTIVE NOTES (Type of report and inclusive dates) Semi-annual report March 15 through September 15, 1971		
5. AUTHOR(S) (First name, middle initial, last name) Aida S. Khalafalla		
6. REPORT DATE September 15, 1971	7a. TOTAL NO. OF PAGES 57	7b. NO. OF REFS 16
8a. CONTRACT OR GRANT NO. H0210026	8b. ORIGINATOR'S REPORT NUMBER(S) 12288-IR1	
8c. PROJECT NO. ARPA order #1579		
8d. PROGRAM CODE 1F10	8e. OTHER REPORT NO(S) (Any other numbers that may be assigned this report)	
10. DISTRIBUTION STATEMENT Distribution of this document is unlimited.		
11. SUPPLEMENTARY NOTES		12. SPONSORING MILITARY ACTIVITY Advanced Research Projects Agency Washington, D.C. 20301
13. ABSTRACT Existing impedance equipment has been modified to measure the complex impedance of rocks in the frequency range of .05 to 2,000 Hz. Impedance measurements have been carried out on samples of Dresser basalt, Charcoal granite and Sioux Quartzite. The resulting series reactance and resistance values have been displayed on an Argand diagram and also, plotted against the logarithm of frequency. Adherence of the data to the circular arc plot is clearly evident. Qualitative effects on impedance were found for both temperature and rock humidity. A method was developed to correct rock impedance data for electrode polarization effects. A technique was developed to extract the rock dielectric constants from the impedance parameters. The real and imaginary parts of the complex dielectric constant for basalt have been displayed on a Cole-Cole plot and also, plotted against the logarithm of frequency.		

DD FORM 1 NOV 57 1473

Unclassified  
Security Classification

14. KEY WORDS	LINK A		LINK B		LINK C	
	ROLE	WT	ROLE	WT	ROLE	WT
Dielectric constant						
Impedance						
Rocks						
Dielectric relaxation						
Temperature						
Moisture						
Computer						
Electrical model						

12288-IR1

15 September 1971

**DIELECTRIC RELAXATION AND ROCK  
GEOPHYSICAL CHARACTERISTICS**

Semiannual Report

15 March through 15 September 1971

Submitted to

U. S. Bureau of Mines (ARPA)  
Contract No. H0210026

Prepared by:

A. S. Khalafalla, PhD  
Senior Principal Research Scientist

Approved by: \_\_\_\_\_

*H. Mocker*

Hans Mocker, PhD  
Supervisor,  
Physical Science Group

Honeywell Inc.  
Systems and Research Center  
Research Department  
2345 Walnut Street  
St. Paul, Minnesota 55113

CONTENTS

	Page	
SECTION I	PROJECT OBJECTIVES	1-1
	Research Objectives for the First Six Months	1-1
	Significant Results	1-1
SECTION II	DESCRIPTION OF EXPERIMENTAL EQUIP- MENT AND TECHNIQUE	2-1
	A. Experimental Setup	2-1
	B. Sample Preparation	2-4
SECTION III	RESULTS AND DISCUSSION	3-1
	A. Impedance Parameters of Dresser Basalt	3-1
	B. Impedance Parameters of Granite	3-4
	C. Impedance Parameters of Quartzite	3-5
	D. Effect of Humidity on Rock Impedance	3-6
	E. Effect of Temperature on Rock Impedance	3-8
	F. Effect of Rock Size and Shape on Its Impedance Diagram	3-15
	G. Electrode Effects	3-16
	H. Transformation of Impedance Parameters to Dielectric Parameters	3-19
	I. Cole-Cole Diagrams - Dielectric and Impedance Parameters of Dresser Basalt	3-25
SECTION IV	TECHNICAL REPORT SUMMARY	4-1
SECTION V	LITERATURE CITED	5-1
APPENDIX A	ELECTRICAL MODELS TO SIMULATE ROCK IMPEDANCE	
APPENDIX B	ELECTRICAL ANALOG WITH ONE FREQUENCY DEPENDENT RESISTANCE	

ILLUSTRATIONS

Figure		Page
1	Computer Display of the Impedance Circular Arc for a Dresser Basalt Sample	1-3
2	Computer Display of the Impedance Circular Arcs for Granite Samples	1-4
3	Computer Display of the Impedance Circular Arc for Large Diameter Quartzite Disc Sample	1-5
4	Schematic of Experimental Setup	2-3
5	Argand Circular-Arc Plot for a Basalt Sample	3-2
6	Dielectric Dispersion and Relaxation of Dresser Basalt	3-3
7	Effect of Moisture on the Impedance Semicircle of Basalt	3-7
8	Variation of Impedance Parameters with Log Frequency for Dresser Basalt (II) at Room Temperature, 22°C	3-10
9	Variation of Impedance Parameters with Log Frequency for Dresser Basalt (II) at 0°C	3-13
10	Specific Impedance Parameters for A - Basalt; B - Granite; and C - Quartzite	3-20
11	Cole-Cole Plot of Dresser Basalt	3-28
12	Dielectric Permittivity of Dresser Basalt as a Function of Frequency	3-29
13	Cole-Cole Plot of Dresser Basalt	3-30
14	Dielectric Permittivity of Dresser Basalt as a Function of Frequency	3-31

TABLES

Table		Page
1	Impedance Data on Basalt (II) at 22°C	3-9
2	Impedance Data on Basalt (II) at 0°C	3-12
3	Electrode Corrections for Basalt	3-18
4	Electrode Corrections for Granite	3-18
5	Impedance and Dielectric Data on Basalt (III)	3-26
6	Impedance and Dielectric Data on Basalt (III)	3-27
7	Electric and Dielectric Parameters of Dresser Basalt	3-32
8	Impedance and Dielectric Data on Quartzite	3-34

## DIELECTRIC RELAXATION AND ROCK GEOPHYSICAL CHARACTERISTICS

### SECTION I PROJECT OBJECTIVES

The ultimate objective is to adopt rock dielectric parameters as indicators of their geophysical characteristics and genesis. To achieve this goal, dielectric relaxation mechanisms in representative rocks must be developed. Electrical models simulating rock dielectric dispersions will be utilized to correlate rock properties with the model parameters. Self- and mutual-impedance data of rocks at a broad frequency range will be gathered.

#### RESEARCH OBJECTIVES FOR THE FIRST SIX MONTHS

The objectives during this period were to modify our existing impedance equipment with its on-line computer capabilities to measure the complex impedance of rocks in the frequency range 0.05 to 2,000 Hz. The next step was to conduct impedance measurements on three selected rock samples provided by the contracting agency and to display the data on an Argand Diagram. A further objective was to develop techniques for the transformation of impedance parameters to dielectric parameters and to construct Cole-Cole plots for a representative rock.

#### SIGNIFICANT RESULTS

An analog/digital computer setup was assembled to evaluate rock impedance in the frequency range 0.05 to 2 kHz. Room temperature measurements

were made on several samples of basalt, granite and quartz. The data appear to verify the impedance circular-arc diagram when displayed in the Argand plane. Figures 1 through 3 show the actual computer output for the impedance components of basalt, granite and quartzite rock samples.

The adherence of the data to the circular-arc plot is clearly evident. Qualitative effects were found for both temperature and rock humidity. A method was developed to correct the rock impedance experimental data for electrode polarization artifacts. A new technique was developed to extract the rock dielectric constants from their corrected and normalized impedance parameters. Detailed results and their analyses are given in Section III of this report. The technical report summary is given in Section IV.

NOT REPRODUCIBLE

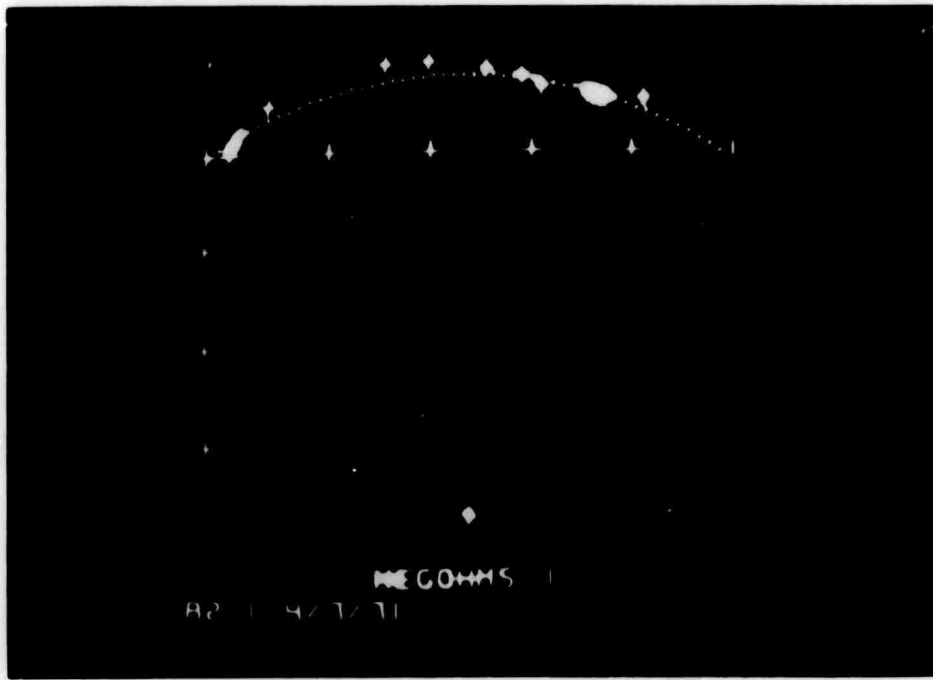


Figure 1. Computer Display of the Impedance Circular Arc for a Dresser Basalt Sample. Points (+) represent experimental variation of reactance with resistance at a given frequency. Dotted curve is an arc of the computer data-filled circle in the least square sense.

NOT REPRODUCIBLE

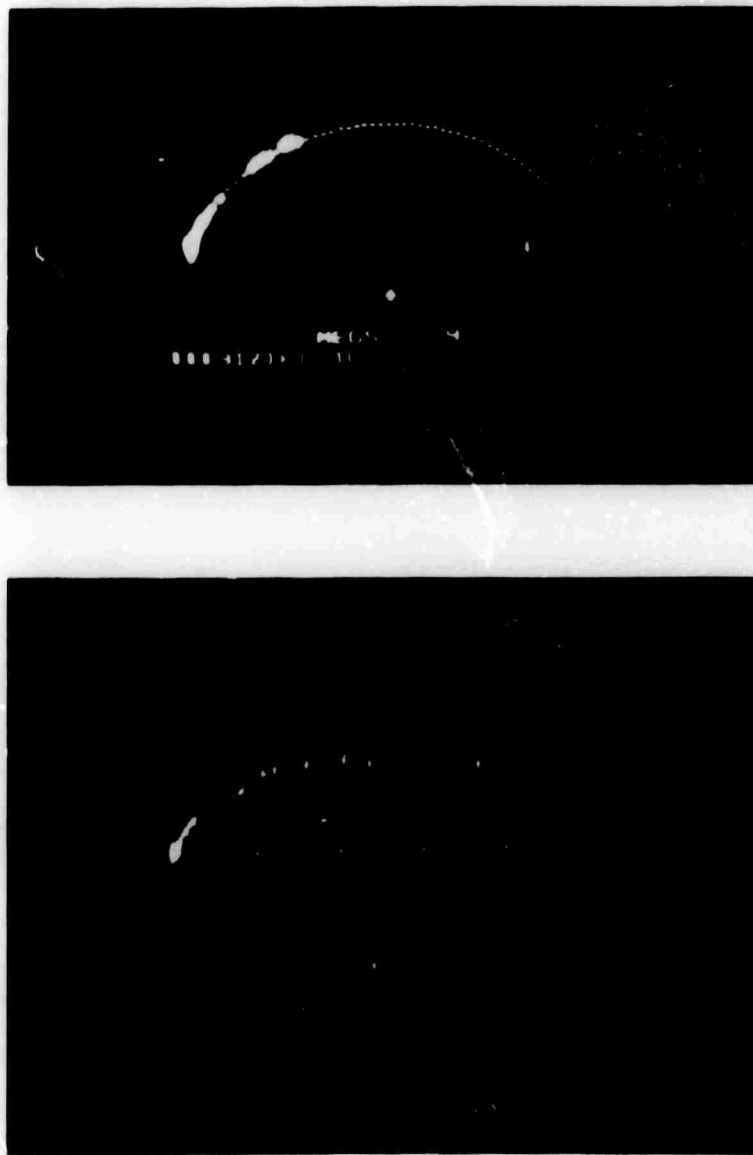


Figure 2. Computer Display of the Impedance Circular Arcs for Granite Samples. Top photograph is for a long granite cylinder (4.41 cm). Bottom photograph is for a thin slice of the granite cylinder (0.15 cm). Points (+) represent variation of reactance with resistance at a given frequency. Dotted curves are arcs of the computer data-fitted circle in the least square sense.

NOT REPRODUCIBLE

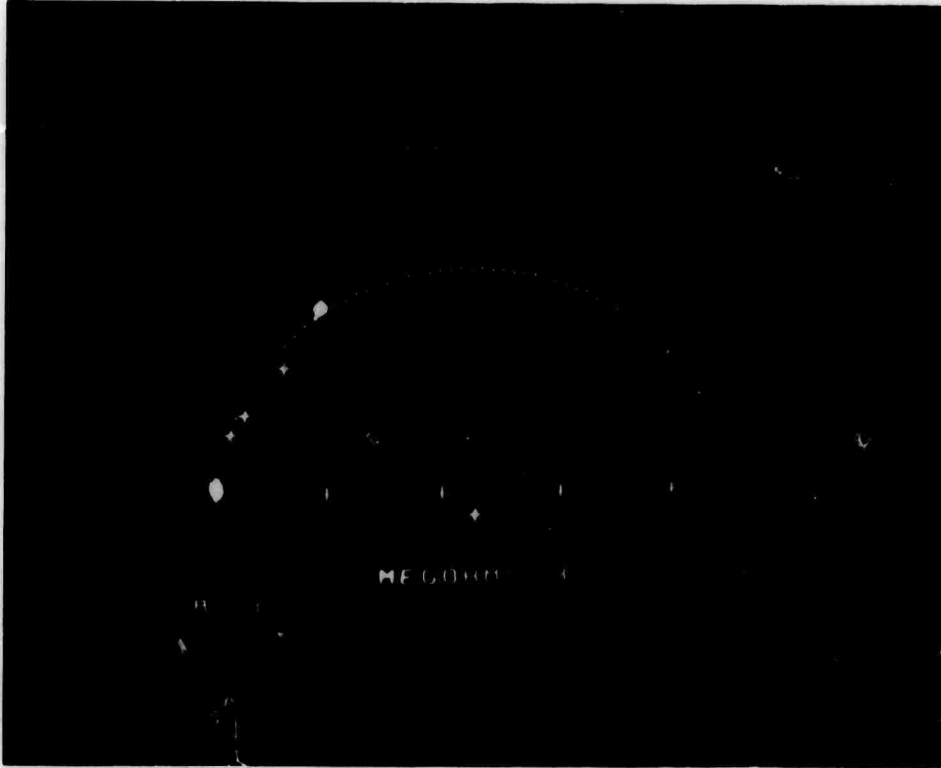


Figure 3. Computer Display of the Impedance Circular Arc for a Large Diameter Quartzite Disc Sample. Points (+) represent experimental variation of reactance with resistance at a given frequency. Dotted curve is an arc of the computer data-fitted circle in the least square sense.

**BLANK PAGE**

## SECTION II

### DESCRIPTION OF EXPERIMENTAL EQUIPMENT AND TECHNIQUE

#### A. EXPERIMENTAL SETUP

The basic approach to the experimental determination of the rock impedance is the use of the rock as a feedback impedance in an operational amplifier. Thus, for a known input signal and resistance, the rock impedance can be determined from the amplifier output signal. This technique lends itself to convenient on-line signal analysis through the use of analog-to-digital conversion equipment.

Figure 4 illustrates the experimental setup in simplified form. Basically, a sinusoid at known frequency drives the amplifier containing the rock, while an in-phase square wave generated simultaneously with the sinusoid is used to clearly define the period of the wave form.

The output from the rock amplifier is sampled over some interval consistent with the signal frequency and converted to digital form. At this state a DDP-24 computer performs a discrete Fourier transform and computes the equivalent series resistance and reactance for the signal.

Included within the analog circuitry is an amplifier having a known fixed (calibration) resistor in its feedback loop. The signal from this amplifier is analyzed simultaneously with the rock signal and provides a reference signal of known amplitude and phase.

Another amplifier is provided just ahead of the calibration amplifier to provide a means of easily changing the gain through the calibration branch without changing the calibration resistor itself.

The raw data is presently extracted as printed values of frequency, series resistance, series reactance, and impedance phase angle. The method of calculating the series resistance and reactance is outlined in the following. The voltage output,  $e_o$  (see Figure 4), from the amplifier having the rock as its feedback impedance, is given by

$$e_o = -Z_R e_i \quad (1)$$

Similarly, the output  $e'_o$  from the calibration amplifier is given by

$$e'_o = - \frac{R_c}{R'_i R''_i} e_i \quad (2)$$

The amplitude of the complex impedance  $Z_R$  is thus given by

$$|Z_R| = \frac{|e_o|}{|e'_o|} \left( \frac{R_c}{R'_i R''_i} \right) \quad (3)$$

where  $e_o$  and  $e'_o$  are determined from a Fourier analysis of the output voltages  $e_o$  and  $e'_o$ .

The Fourier analysis also provides the phase angle  $\phi$  between output voltage and current. Thus the series resistance and reactance are calculated from

$$R_s = |Z_R| \cos \phi, \text{ and } X_s = |Z_R| \sin \phi$$

A least square circle fit is also automatically made for the  $R_s$  and  $X_s$  data and displayed along with the  $R_s$  and  $X_s$  data on a CRT screen. In addition, all data are permanently stored on magnetic tape for future call back.

Detailed description of the computer programs and electronic circuitry used in this work can be found in reference (1).

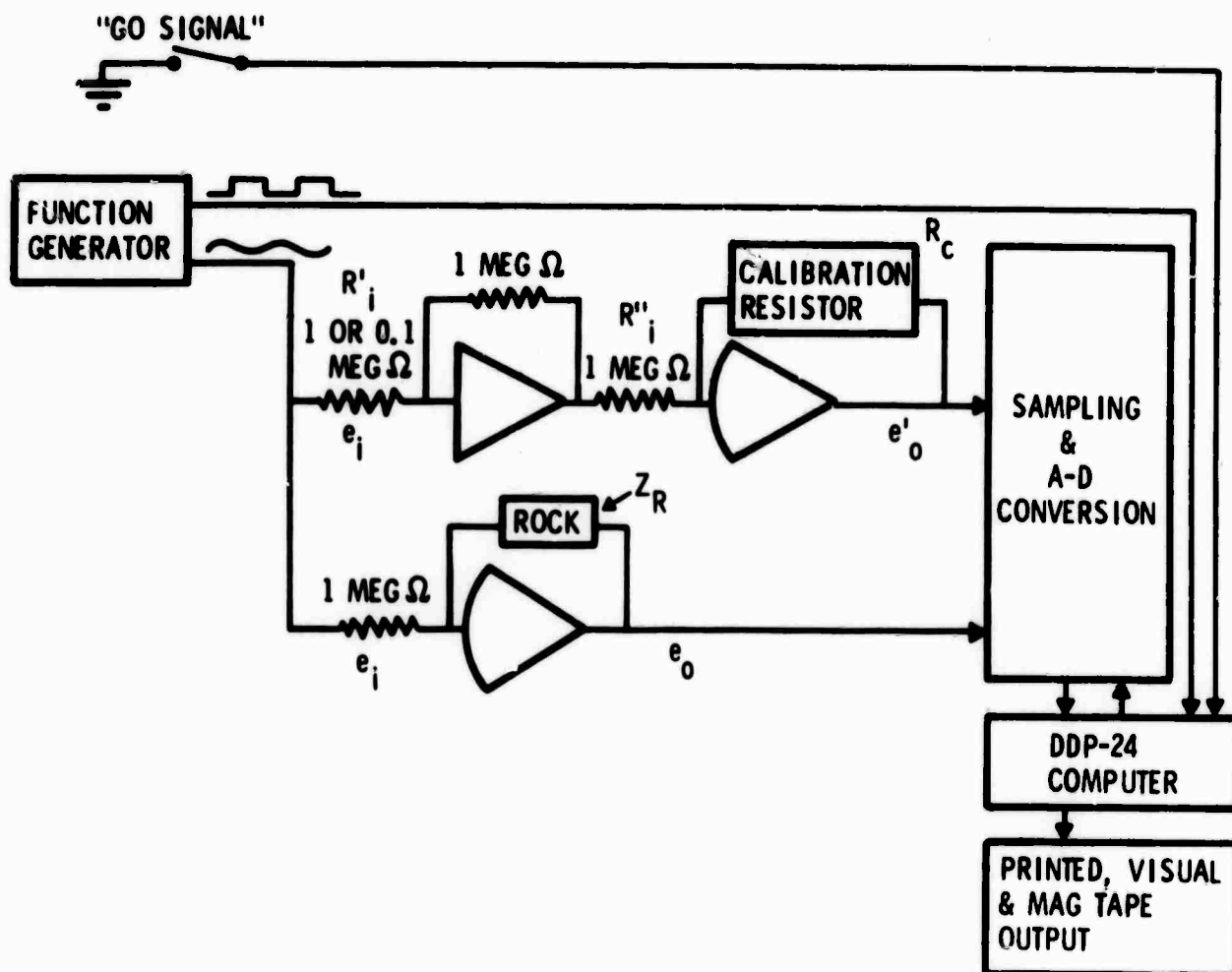


Figure 4. Schematic of Experimental Setup

## B. SAMPLE PREPARATION

With the exception of the application of electrode material, all measurements to date have been made on rocks "as received" from the customer.

The electrodes are applied to the flat surfaces of the cylindrical samples. An epoxy-based conductive adhesive\* is applied in a thin coat and allowed to dry for at least two days at room temperature.

Copper leads made from thin sheet stock are laid on top of the electrode material and the rock is clamped tightly between two plates of printed circuit board to secure even electrical contact with the rock.

---

\* Eccobond Solder V-91, Emerson & Cumming, Inc.  
Dielectric Materials Division, Canton, Massachusetts.

### SECTION III RESULTS AND DISCUSSION

#### A. IMPEDANCE PARAMETERS OF DRESSER BASALT

A disc basaltic sample (I) containing  $\text{SiO}_2$ ,  $\text{Fe}_3\text{O}_4$ ,  $\text{Al}_2\text{O}_3$ ,  $\text{TiO}_2$ ,  $\text{CaO}$  and  $\text{MgO}^*$  in the percents 48.42, 6.6, 15.23, 1.9, 8.35 and 6.4 percent, respectively, and measuring 0.635 cm in length and  $6.41 \text{ cm}^2$  in cross section was supplied to Honeywell by the Thermal Fragmentation Group, Twin Cities Mining Research Center, U.S. Bureau of Mines. Silver electrodes were painted to the circular surfaces of the rock and contact to the electrodes was made with copper wires. Replication of the impedance data at 14 different frequencies and at time intervals ranging from several minutes to three weeks, as well as with repeated electrode applications to the cleaned rock surface, gave fairly reproducible results. The standard deviation at the high frequency of 2 KHz was 3.8 percent of the mean in  $R_s$ , and 2.6 percent of the mean in  $X_s$ . At the low frequency of 0.05 Hz, standard deviations of 3.7 and 8.1 of the mean in  $R_s$  and  $X_s$ , respectively, were calculated.

The reactive component of the measured impedance is plotted in Figure 5 against its corresponding resistive component at a series of frequencies. The least-squares circle fit to the data was determined and plotted in the solid arc of Figure 5. The experimental points were found to deviate from the fitted arc by a standard deviation of 2.44 percent of the fitted radius. Inspection of the data in Figure 5 suggests a value of 16.4 megohm for the d-c resistance,  $R_o$ , of this basalt sample. A rock phase angle,  $\phi$ , of 29 degrees was also measured for this sample.

When the data was displayed in a log frequency plot, Figure 6 was obtained. Curves A and B have been drawn through the series reactance and resistance

\*Chemical analysis of the rock samples are taken from a recent report by Lindroth and Kranze (reference 2).

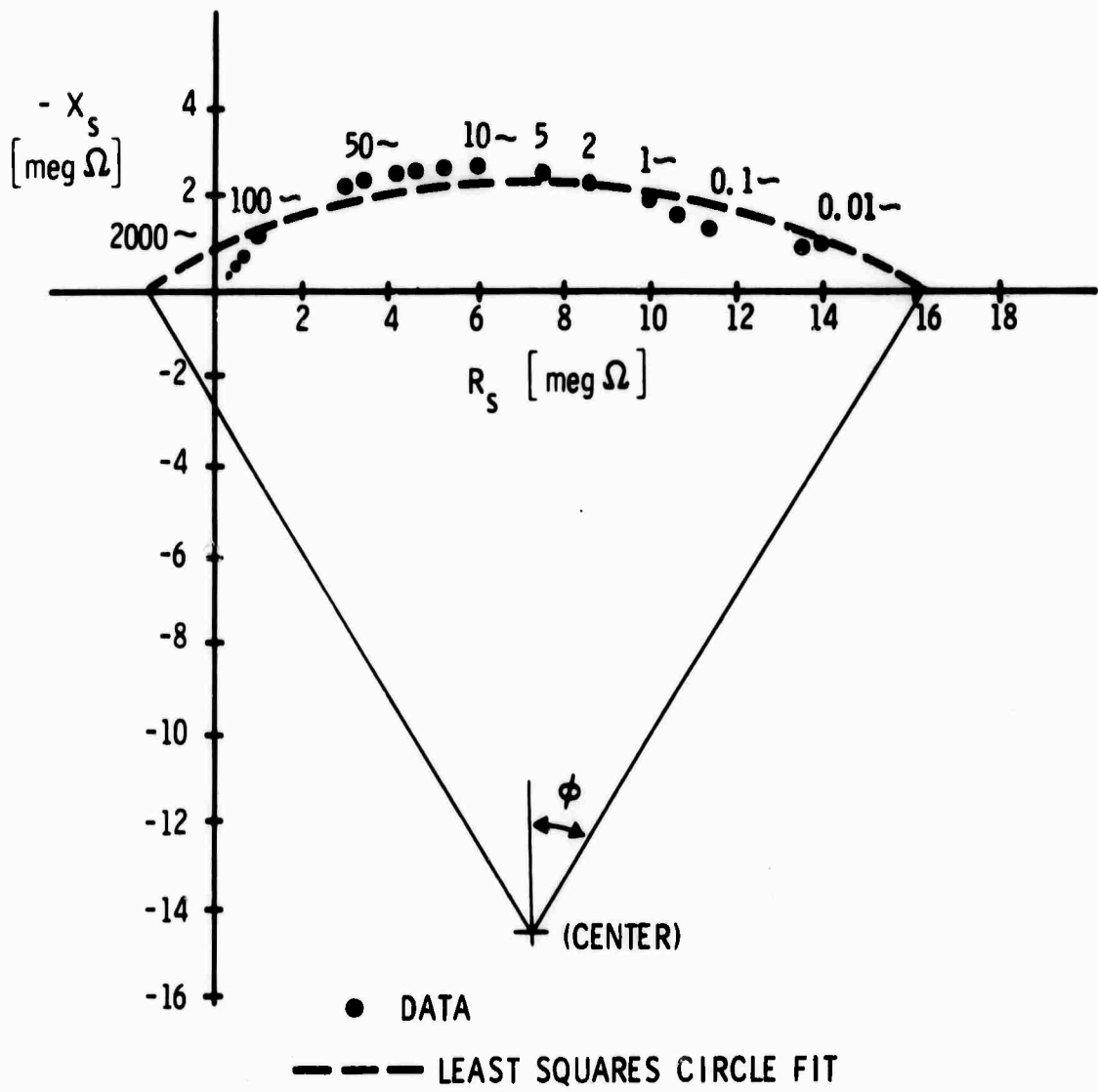


Figure 5. Argand Circular-Arc Plot for a Basalt Sample

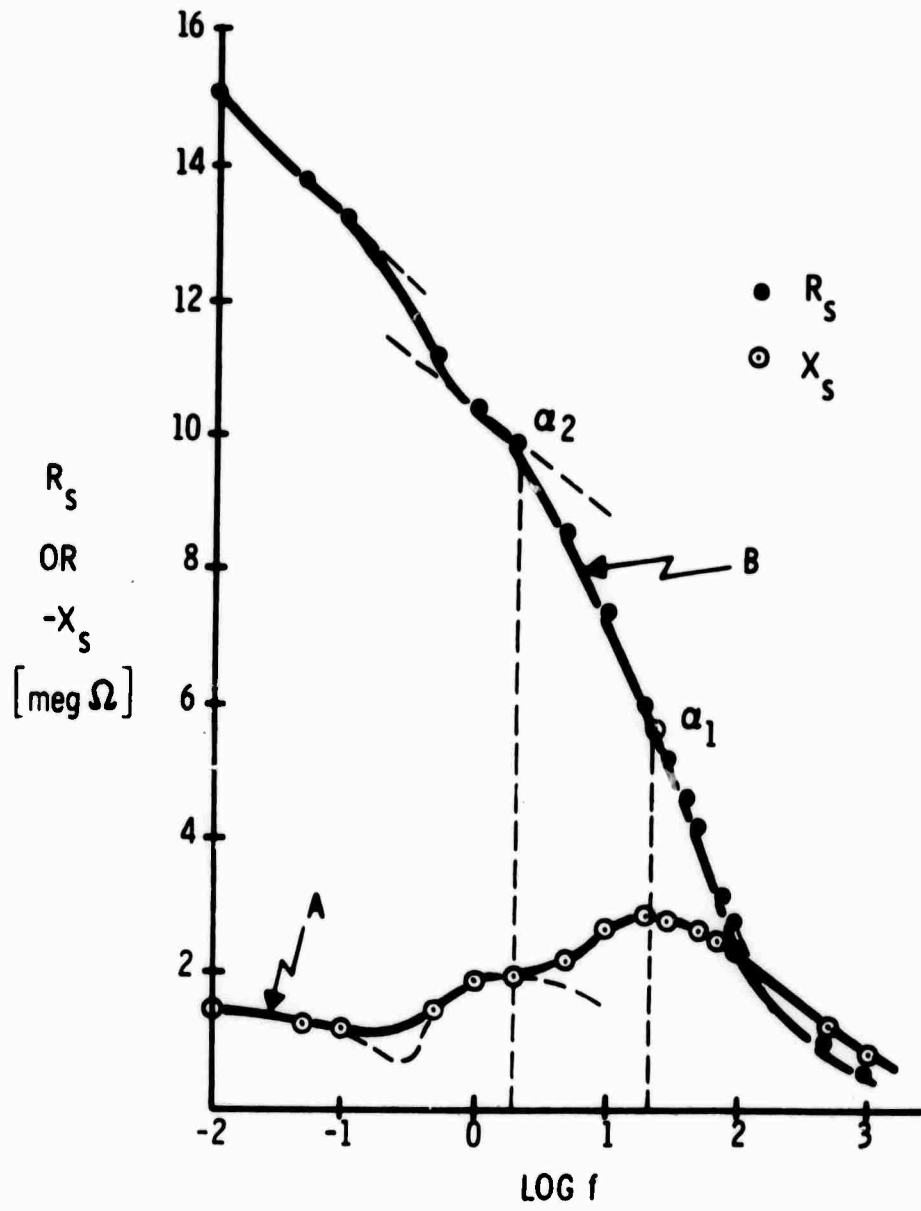


Figure 6. Dielectric Dispersion and Relaxation of Dresser Basalt

data, respectively. Careful examination of these curves indicates three dielectric relaxation peaks. The main peak appears at a frequency of 21.8 Hz, which corresponds to a turnover frequency,  $\omega_{\max}$ , of 136.9 radians per second, and to a relaxation time,  $\tau$ , of 7.3 milliseconds. A second well-developed relaxation peak appears at a frequency of 1.7 Hz, corresponding to a relaxation time of 93.4 milliseconds. A third relaxation peak appears to be anticipated at frequencies less than 0.01 Hz. In agreement with these observations, the  $R_s$  curve shows two definite dispersion regions.

The first dispersion,  $\alpha_1$ , appears at a frequency which coincides with the first and main relaxation peak in the series reactance. A second dispersion,  $\alpha_2$ , occurs at a frequency of 0.05 Hz, somewhat displaced from the second relaxation peak. A third dispersion may be anticipated at frequencies below 0.01 Hz. In conformity with the adopted notations in dielectric dispersion, we will reserve the symbol  $\alpha$  for rock dielectric dispersion in the low-frequency range (below 10 KHz). The symbol  $\beta$  will be used for dispersions in the medium frequency range; i. e., between 10 KHz and 100 megahertz. The symbol  $\gamma$  will be adopted for dispersions at frequencies beyond the 100 megahertz. Each of these dispersions may split into more than one sub-dispersion, such as the  $\alpha_1, \alpha_2, \dots$  etc., of the  $\alpha$ -dispersion investigated in this project. Each of the discovered dispersions should correspond to a certain relaxation mechanism of a substructure "structon" within the rock. Huggins (Reference 3) recommended the use of local structural groupings as the basic structural units. He used the term "structon" to signify a specific type of atom(s), with specific kinds and numbers of close neighbors.

## B. IMPEDANCE PARAMETERS OF GRANITE

A sample of charcoal gray granite from St. Cloud, Minnesota, was supplied to Honeywell by personnel from the Thermal Fragmentation Group of the Twin Cities Mining Research Center. The sample analyzed (Reference 2)

63.5 percent  $\text{SiO}_2$ , 15.6 percent alumina, 4.1 percent CaO, 3.6 percent  $\text{Na}_2\text{O}$ , 3.6 percent  $\text{K}_2\text{O}$ , 4.2 percent CaO, 2.7 percent FeO, 1.8 percent  $\text{Fe}_2\text{O}_3$  and smaller quantities of manganese and titanium.

The impedance data of granite followed the same pattern as that of basalt, except that the semicircular arc was not easy to close at the low-frequency side. Resistive and reactive components for a cylindrical granite sample 0.148 cm in length and  $3.67 \text{ cm}^2$  in cross-sectional area described a segment of a circular arc when plotted in an Argand diagram. Computer extrapolation of this arc to its point of intersection with the resistive axis yielded a value of  $4.8 \times 10^9$  ohm (about 5 gigaohm) for  $R_0$ . The preceding basaltic sample has an  $R_0$  value of 16.4 megohm. If a basalt sample of the same dimensions of granite had been used, its  $R_0$  value would be

$$16.4 \left( \frac{0.635}{0.148} \right) \div \left( \frac{6.41}{3.67} \right) = 40.5 \text{ megohm}$$

The d-c resistance value,  $R_0$ , as determined by extrapolation of the impedance vector to zero frequency, is therefore about a hundred times higher for granite than for basalt of similar shape and dimensions. This result is consistent with the fact that granite contains 30 percent more of the covalently coordinated, and hence nonconductive, silica tetrahedra. Basalt has more iron, calcium and titanium, although somewhat less sodium and potassium than granite.

### C. IMPEDANCE PARAMETERS OF QUARTZITE

Sioux quartzite, with a bulk density of  $2.64 \text{ gram cm}^{-3}$ , was used in the following experiments. The source location of this type of quartzite was Jaspar, Minnesota. Its chemical analysis (Reference 2) indicated 97.84 percent silica, 0.87 percent  $\text{Al}_2\text{O}_3$ , 0.81 percent CaO, 0.25 percent FeO and 0.27 percent  $\text{Fe}_2\text{O}_3$ . As with granite, the impedance parameters of quartzite were very large, in the gigaohm range, at low frequencies. A quartzite disc sample of

length 0.61 cm and cross-sectional area 18.8 cm<sup>2</sup> gave an extrapolated  $R_o$  value of  $4.5 \times 10^9$  ohms. When corrected to the same dimensions of granite, this value should be modified to

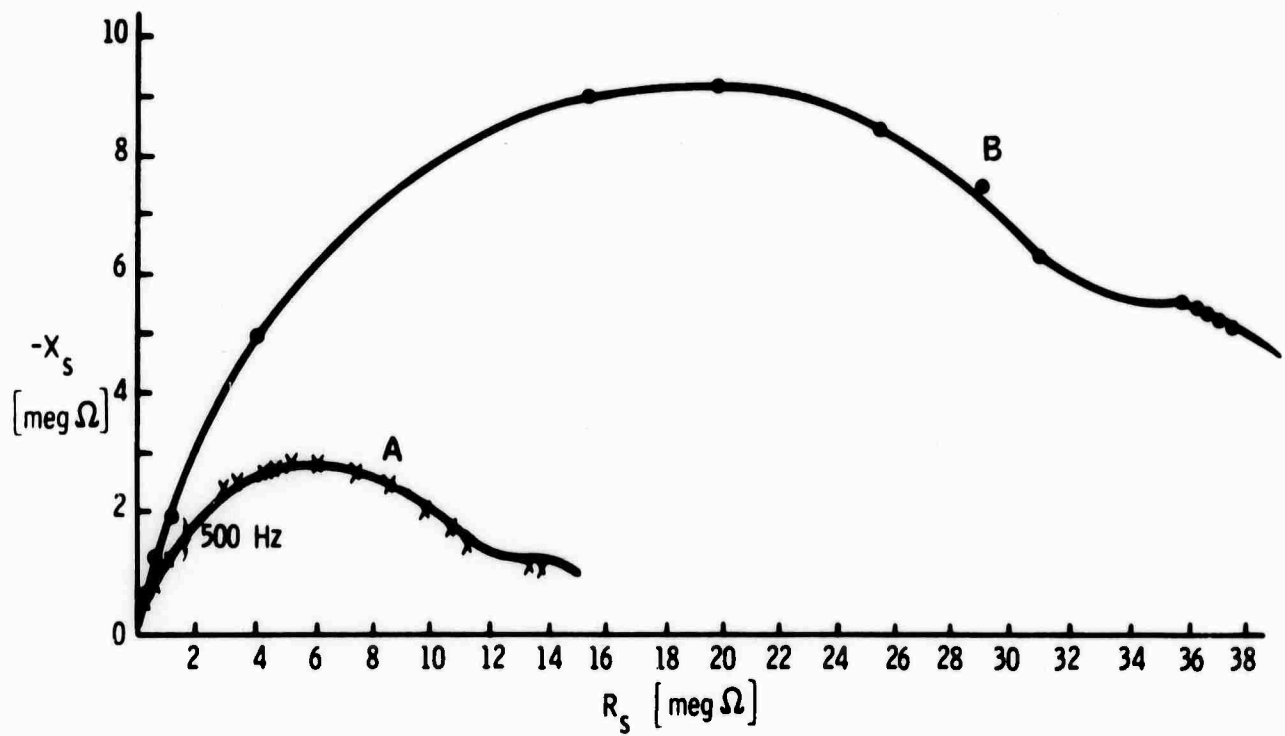
$$4.5 \times 10^9 \left( \frac{0.148}{0.61} \right) \div \left( \frac{3.67}{18.8} \right) = 5.6 \times 10^9 \text{ ohms}$$

Hence, the quartz d-c resistance is about 20 percent higher than that of granite, and still more than two orders-of-magnitude higher than that of basalt. Thus it appears that a rock's impedance parameters are not only affected by the amount of silica it contains, but also by the amounts of volatile alkali oxides within the rock.

#### D. EFFECT OF HUMIDITY ON ROCK IMPEDANCE

The effect of moisture content has been examined with the basaltic sample (I) and the data are shown in Figure 7. Curve A in this figure was obtained with the rock sample as received from the customer with no attempt made to control the rock environment. Curve B in Figure 7 was obtained when the basalt sample was baked with electrodes attached in a 110°C oven for 19 hours. After baking, the sample was immediately placed in an airtight desiccator and allowed to cool to room temperature for the following 24 hours. The resulting measurements indicated a significant increase in impedance at frequencies up to 500 Hz. Above 500 Hz, the humidity effect on impedance parameters is not very pronounced. While the  $R_o$  value for the unbaked basalt was 16.4 megohm, the value determined when the rock was baked is about 45 megohm.

Chemical analysis of Dresser basalt (Reference 2) indicated the presence of 0.14 percent water in the rock and a loss on ignition (LOI) of 2.26 percent. By contrast, the granite sample and the quartzite sample contained 0.11 and 0.08 percent water, respectively, and showed a loss on ignition of 0.59 and 0.32 percent, respectively. Upon ignition, not only water is lost, but some



A - Rock at ambient room environment

B - Dry baked rock in desiccator

Figure 7. Effect of Moisture on the Impedance Semicircle of Basalt

of the volatile oxides such as  $\text{Na}_2\text{O}$  and  $\text{K}_2\text{O}$  may also sublime. When these volatile oxides are attached to the nonvolatile silica tetrahedron, they are in the form of a solid solution of alkali silicate, and the alkali will thereby be prevented from sublimation. A free alkali metal oxide unit in the rock will show a higher LOI, and will also be easily leachable with water, and thus will contribute significantly to the rock conductivity. Thus the alkali content of a rock as shown by chemical analysis will not be the decisive factor in determining the rock conductivity; rather, the mode by which the alkali oxide enters the rock structure will play the predominant role. Because of its higher LOI, Dresser basalt appears to have more of the mobile sodium and potassium ions which contribute greatly to its higher conductivity.

#### E. EFFECT OF TEMPERATURE ON ROCK IMPEDANCE

Experiments were performed on basalt to determine the effect of temperature on rock impedance as a preliminary for a research proposal on "Effect of Frequency and Temperature on Rock Dielectric Parameters," which was recently submitted to ARPA and the U.S. Bureau of Mines. The basaltic sample (II) used in this experiment was a large circular disc 0.54 cm in thickness and 5.21 cm in diameter. It differed from the Dresser basalt (I) used previously in both color and grain size. The new sample was darker in its greenish tint than the former. The change in texture may be attributed to different phase of rock formation (Reference 4). Impedance has been measured at both room temperature ( $22^\circ\text{C}$ ) and the melting point of ice ( $0^\circ\text{C}$ ). At the low frequency of 0.1 Hz, the impedance at the ice point is considerably higher than that at room temperature. As the frequency increases, the temperature effect becomes less pronounced. Table 1 gives the resistive and reactive impedance components at room temperature and at nominal frequencies ranging from 0.1 to 2000 Hz. The variation of the series reactance at room temperature,  $X_s$ , with log frequency is shown as curve A of Figure 8, while curve B shows the variation of the rock series resistance,  $R_s$ . Both

Table 1. Impedance Data on Basalt (II) at 22°C

LAST RECORD IS T4- 2 4/23/71  
ZEEGO MOD I

B6-1 4/26/71

ENTER RCAL/UNITS  
2μ.  
MEGS

FRQ	RES	RAEC	PHI
μ.09	32.0651	-3.5772	-6.25
μ.5μ	26.5789	-4.54μ7	-9.7μ
μ.99	24.472μ	-5.3178	-12.26
2.μμ	21.8μ83	-6.1671	-15.79
5.μ2	17.6153	-7.μ98μ	-21.95
7.95	15.2352	-7.2887	-25.57
9.96	14.μ585	-7.2972	-27.43
14.97	11.9454	-7.1662	-3μ.96
2μ.μ2	1μ.4838	-6.9575	-33.57
3μ.μ3	8.5419	-6.5137	-37.33
4μ.16	7.2568	-6.11μ3	-4μ.1μ
5μ.1μ	6.3452	-5.7679	-42.27
99.5μ	4.μ188	-4.5μ73	-48.28
2μμ.27	2.3545	-3.2393	-53.99
5μ3.36	1.1232	-1.8585	-58.86
998.19	μ.6598	-1.1528	-6μ.22
2μ22.μ6	μ.4μ74	-μ.654μ	-58.μ8

17 SAMPLES

CIRCLE CENTER = 16.9612 2μ.4344  
RADIUS = 27.6828  
ERROR μ.88188 REDUCED TO μ.58838  
IN 17 STEPS

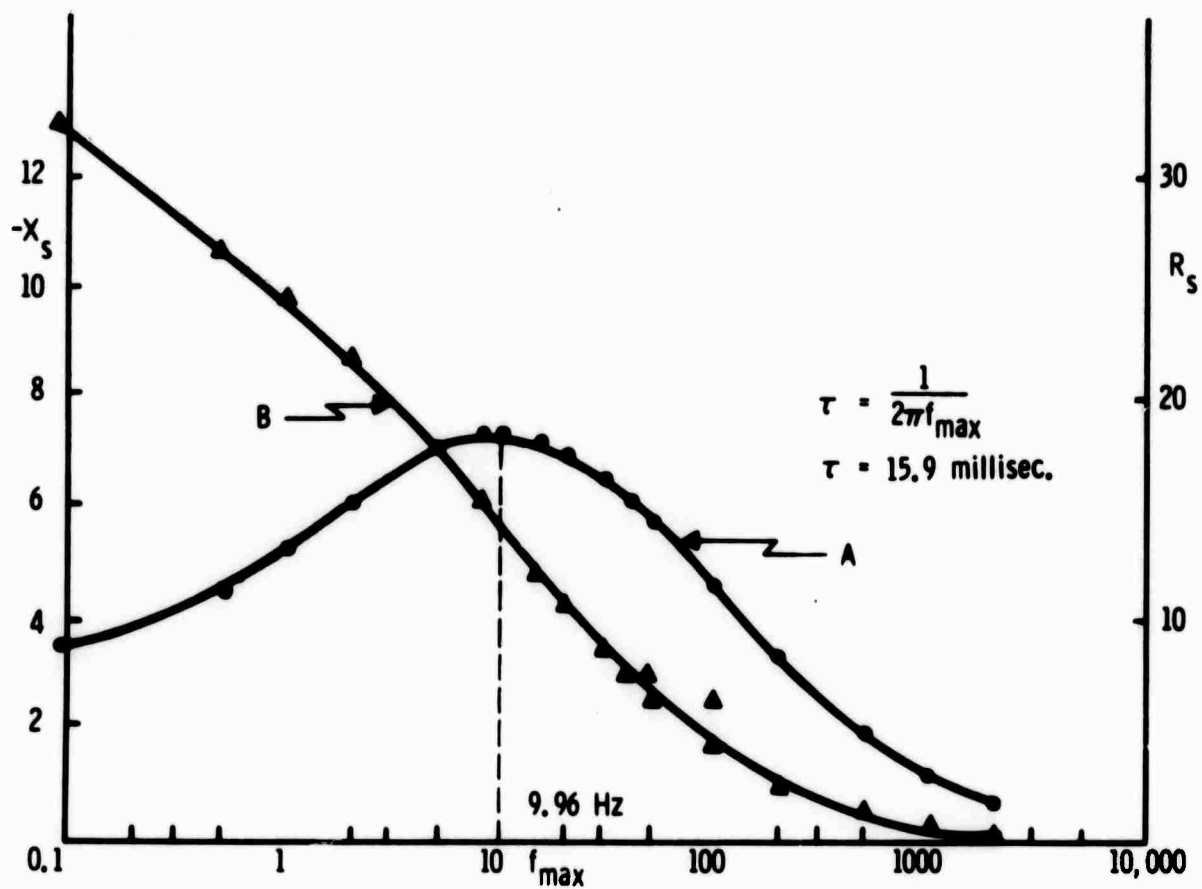


Figure 8. Variation of Impedance Parameters with Log Frequency for Dresser Basalt (II) at Room Temperature, 22°C

curves indicate a turnover frequency,  $f_{\max}$ , of 9.96 Hz, which corresponds to a room temperature relaxation time,  $\tau$ , of

$$\tau = \frac{1}{\omega_{\max}} = \frac{1}{2\pi f_{\max}} = 15.9 \text{ milliseconds}$$

When the previous experiment was repeated at the melting point of ice, the data in Table 2 were obtained. Variation of the impedance parameters, at room temperature with log frequency, is shown in Figure 9, where a turnover frequency,  $f'_{\max}$ , of 9.96 Hz is determined. At 0°C, the relaxation time is given by

$$\tau' = \frac{1}{2\pi f'_{\max}} = 79.5 \text{ milliseconds}$$

The rock d-c resistance,  $R_o$ , at 0°C is 191.8 megohms, which should be compared to the room temperature value of 37.3 megohm. Thus both rock d-c resistance and relaxation time decrease significantly with rise in temperature. At higher frequencies, the temperature effect becomes less pronounced.

According to Eyring's theory (Reference 5) of absolute reaction rates, the turnover or characteristic frequency is equal to the universal frequency ( $kT/h$ ), modified by a free energy of activation term, thus

$$f_{\max} = \left(\frac{kT}{h}\right) e^{-\Delta F^\dagger/RT} \quad (4)$$

where  $k$  is Boltzmann's constant,  $T$  is the absolute temperature,  $\Delta F^\dagger$  is the free energy of activation per mole of the relaxing unit within the rock matrix, and  $R$  is the molar gas constant.

If it is assumed that the silica tetrahedral unit is the unit structure responsible for the relaxation mechanism, then a mole of the relaxing units ( $\text{SiO}_4$ ) will be 92 grams of the rock. The free energy of activation is related to the enthalpy of activation,  $\Delta H$ , per mole of relaxing units by

Table 2. Impedance Data on Basalt (II) at 0°C

## CRT CALIBRATION

DATA TAPE ON UNIT 2 - PUSH START

\*\*\*\*\* PAUS \*\*\*\*\*

LAST RECORD IS B6-1 4/26/71

ZEEGO MOD I

B7-1 4/26/71

ENTER KCAL/UNITS

2μ.

MEGS

FRQ	RES	RAEC	PHI
μ.μ9	16μ.3149	-26.5281	-9.4μ
μ.5μ	11μ.55μ9	-36.20μ7	-18.16
μ.99	92.3657	-39.287μ	-23.μ4
2.μμ	72.3747	-39.8985	-28.87
5.μμ	47.1312	-36.μ387	-37.41
7.96	35.9375	-32.25μ4	-41.91
9.95	31.1345	-3μ.1291	-44.μ6
2μ.μ2	19.μμ96	-22.9683	-5μ.39
3μ.μ8	13.8184	-18.9881	-53.96
4μ.23	1μ.8μ11	-16.3439	-56.54
5μ.μ5	8.8994	-14.4474	-58.37
99.5μ	4.71μ5	-9.4347	-63.47
2μμ.27	2.3633	-5.7473	-67.65
5μ4.2μ	μ.9996	-2.7933	-7μ.32
998.19	μ.57μμ	-1.5737	-7μ.1μ
2μ18.35	μ.3682	-μ.8424	-66.4μ

16 SAMPLES

CIRCLE CENTER = 91.5μ41 87.5214  
 RADIUS = 129.8529  
 ERROR 5.15521 REDUCED TO 2.35518  
 IN 11 STEPS

12288-IR1

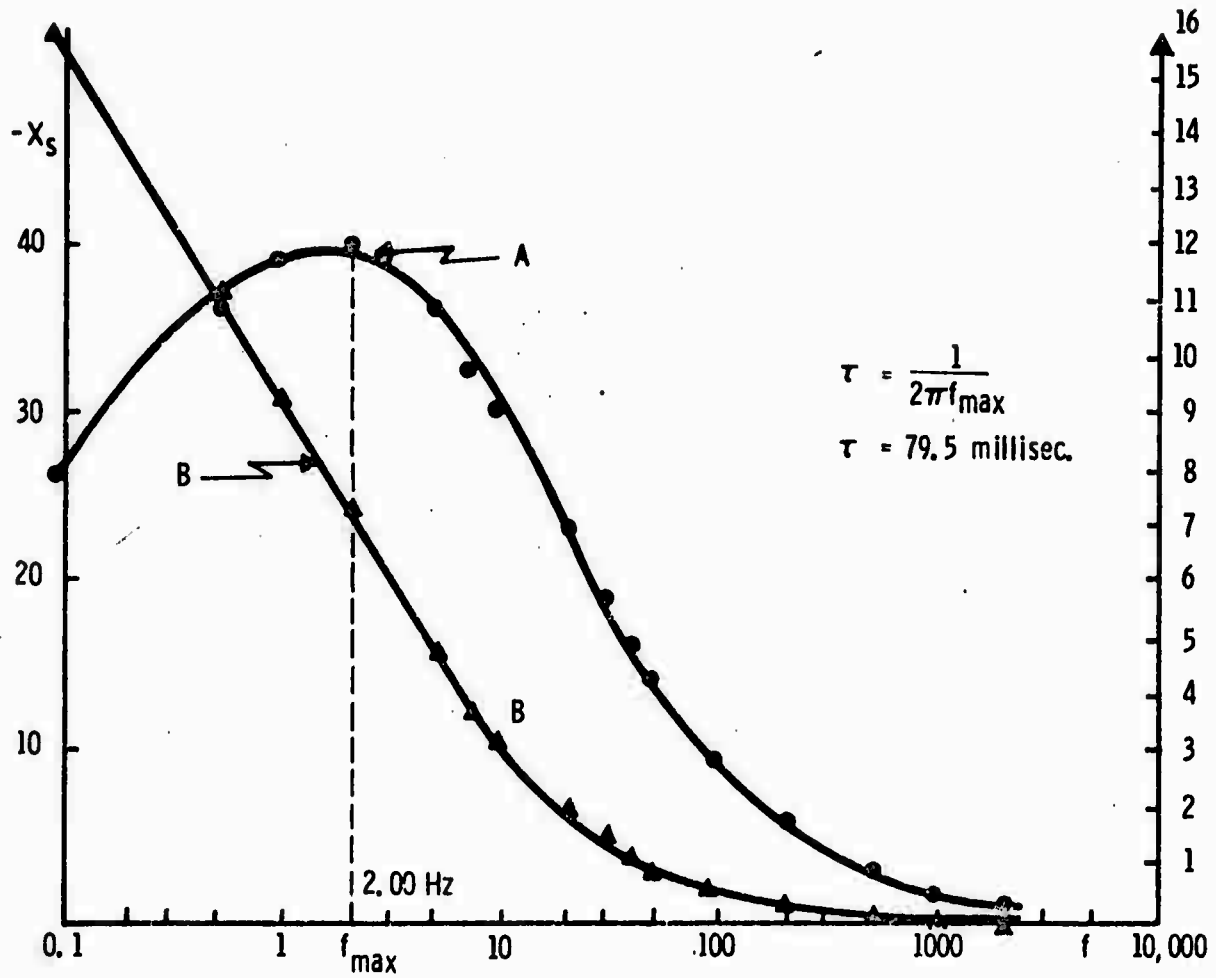


Figure 9. Variation of Impedance Parameters with Log Frequency for Dresser Basalt (II) at 0°C

$$\Delta F^\ddagger = \Delta H^\ddagger - T\Delta S^\ddagger \quad (5)$$

where  $\Delta S^\ddagger$  is the entropy of activation. Applying Equation (5) into (4), one obtains

$$f_{\max} = \left( \frac{kT}{h} \right) e^{\Delta S^\ddagger/R} e^{-\Delta H^\ddagger/RT} \quad (6)$$

or

$$\ln (f_{\max}/T) = \ln \frac{k}{h} + \frac{\Delta S^\ddagger}{R} - \frac{\Delta H^\ddagger}{RT} \quad (7)$$

Normally one determines  $f_{\max}$  at a series of temperatures and establishes the validity of the foregoing equations by ascertaining that the plot of  $\ln (f_{\max}/T)$  against  $(1/T)$  is linear. From the slope of this linear plot one determines the enthalpy or heat of activation,  $\Delta H^\ddagger$ , thus

$$\text{Slope} = \frac{\Delta H^\ddagger}{R} \quad (8)$$

and from the intercept of the linear plot with the ordinate, one can determine the entropy of activation,  $\Delta S^\ddagger$ , thus

$$\text{Intercept} = \ln \left( \frac{k}{h} \right) + \frac{\Delta S^\ddagger}{R} \quad (9)$$

Applying Equation (6) to the two datum obtained in this preliminary work, and remembering that  $T = 295^\circ\text{K}$  for room temperature ( $22^\circ\text{C}$ ), and  $T = 273^\circ\text{K}$  for the ice point, then

$$\frac{(f_{\max}/T)}{(f'_{\max}/T')} = e^{-\Delta H^\ddagger \left( \frac{1}{T} - \frac{1}{T'} \right)}, \text{ or}$$

$$\ln \left[ \frac{f_{\max} T'}{f'_{\max} T} \right] = \frac{\Delta H^\ddagger}{R} \left[ \frac{1}{T'} - \frac{1}{T} \right] \quad (10)$$

The enthalpy of activation,  $\Delta H^\ddagger$ , is calculated from Equation (10), thus

$$\begin{aligned} \Delta H^\ddagger &= 2.303R \frac{TT'}{(T - T')} \log \left[ \frac{f_{\max} T'}{f'_{\max} T} \right] \\ &= 2.303 \times 1.987 \times \frac{295 \times 273}{22} \log \left[ \frac{9.96 \times 273}{2.0 \times 295} \right] \\ &= 10,700 \text{ calories or } 10.7 \text{ Kcal.} \end{aligned}$$

Hence, it is estimated that the activation energy for the relaxation process in basalt is about 11 Kcal per mole of relaxing units, or about 0.5 ev (1 ev = 23.05 Kcal/mole).

Future work in this project will further develop this temperature effect and utilize it to compute both the enthalpy and entropy of activation.

#### F. EFFECT OF ROCK SIZE AND SHAPE ON ITS IMPEDANCE DIAGRAM

Experiments on Dresser basalt samples of various sizes and shapes showed significant variations, particularly at the low-frequency end. When the sample was in the form of a long cylinder, reasonable agreement was obtained in the specific impedance values; i. e., the rock specific resistance  $\rho$ , and specific reactance,  $\chi$ . These values were obtained from the measured resistance,  $R$ , and reactance,  $X$ , by multiplying into  $(A/d)$ , where  $A$  is the electrode area and  $d$  is the length of the sample, or the distance between the electrodes. However, with some of these long samples the impedance values at low frequencies

were so high that measurements were difficult at lower frequencies (below 100 Hz) due to amplifier saturation. Upon resorting to thinner samples, the electrode polarization effects were quite substantial and constituted a significant part of the measured impedance especially at low frequency. Similar findings were reported by Takashima and Schwan (Reference 4).

#### G. ELECTRODE EFFECTS

Thin slices were cut from a long cylindrical rock sample. The same electrode material was applied to both sides of the rock sample (with the longer length  $d$ , and for the thinner rock sample whose length was  $d'$ ). The total impedance measured with either rock sample is

$$Z_m = Z + Z_e \quad (11)$$

where  $Z_m$  is the measured impedance,  $Z$  is the true impedance of the rock, and  $Z_e$  is the electrode impedance. For the long sample,

$$Z = \xi \left( \frac{d}{A} \right) \quad (12)$$

and for the thin sample,

$$Z' = \xi \left( \frac{d'}{A} \right) \quad (13)$$

where  $\xi$  is the rock impedivity and  $A$  is the electrode area. Impedivity  $\xi$  is the vector summation of resistivity  $\rho$  and specific reactance  $\chi$ , thus

$$\xi = \rho + j\chi \quad (14)$$

By separating the real from the imaginary variables, identical relationships to those derived for  $Z_e$  will result for electrode resistance  $R_e$  and reactance  $X_e$ . Substituting from (12) and (13) into (11), one obtains for the long sample

$$Z_m = \xi \left( \frac{d}{A} \right) + Z_e \quad (15)$$

and for the thin sample

$$Z_m' = \xi \left( \frac{d'}{A} \right) + Z_e \quad (16)$$

therefore,

$$\frac{Z_m - Z_e}{Z_m' - Z_e} = \frac{d}{d'} = \alpha \quad (17)$$

where  $\alpha$  is the ratio of the lengths of the two rock samples. Solving Equation (17) for  $Z_e$ , one obtains:

$$Z_e = \frac{\alpha Z_m' - Z_m}{(\alpha - 1)} \quad (18)$$

Separating Equation (18) into its real and imaginary parts gives

$$R_e = \frac{\alpha R_m' - R_m}{(\alpha - 1)} \quad (19)$$

and

$$X_e = \frac{\alpha X_m' - X_m}{(\alpha - 1)} \quad (20)$$

A thin slice of height 0.152 cm was cut from a basaltic cylindrical sample (III). The length of the remaining long cylinder was 4.08 cm. Hence,  $\alpha = 26.8$ . Circular silver paste electrodes, each of area  $3.75 \text{ (cm}^2\text{)}$  were fastened to each side of the two cylinders. The impedance data measured on these two rock specimens are shown in columns 2, 3, 4 and 5 of Table 3.  $R_e$  and  $X_e$  calculated from these data with the aid of Equations (19) and (20) are given in columns 6 and 7 of Table 3.

Table 3. Electrode Corrections for Basalt

Frequency (Hz)	Long Cylinder		Small Disc		Electrode		Corrected Cylinder		Corrected Disc		$\rho = (R_S - R_e) \frac{A}{d}$	$\chi = (X_S - X_e) \frac{A}{d}$
	R <sub>S1</sub>	-X <sub>S1</sub>	R <sub>S2</sub>	-X <sub>S2</sub>	R <sub>e</sub>	-X <sub>e</sub>	R <sub>S1</sub> -R <sub>e</sub>	-(X <sub>S1</sub> -X <sub>e</sub> )	R <sub>S2</sub> -R <sub>e</sub>	-(X <sub>S2</sub> -X <sub>e</sub> )		
							$\rho$	$\chi$				
0.502	4059.23	2854.57	164.63	66.46	12.90	-42.17	4046.32	2896.74	151.74	108.63	37.10	26.56
0.995	2661.09	2455.49	130.13	70.75	31.52	-22.16	2629.57	2477.65	98.61	92.91	24.11	22.72
2.00	1731.15	2085.56	95.27	70.44	31.53	-8.07	1699.62	2093.63	63.74	78.51	15.59	19.20
4.02	936.03	1441.44	63.12	59.37	29.10	5.53	906.93	1435.91	34.01	53.85	8.32	13.17
6.03	652.76	1152.74	48.42	52.24	24.88	9.36	627.88	1143.37	23.55	42.88	5.76	10.48
9.95	407.08	831.64	57.48	70.53	43.86	40.88	365.22	790.76	13.62	29.55	3.33	7.25
20.06	286.68	493.78	19.71	29.22	9.31	11.12	277.38	482.65	10.40	18.10	2.54	4.43
50.15	123.52	293.68	9.48	16.99	5.03	6.21	118.49	287.46	4.44	10.78	1.09	2.64
99.50	46.56	200.34	5.26	10.83	3.65	3.45	42.91	196.59	1.61	7.38	0.39	1.81
504	6.13	45.59	1.34	3.20	1.16	1.55	4.97	44.04	0.19	1.65	0.05	0.40
1000	3.64	23.48	0.83	1.83	0.72	0.99	3.12	22.44	0.12	0.84	0.03	0.21
2026	2.93	11.91	0.48	0.97	0.39	0.54	2.55	11.37	0.10	0.43	0.02	0.10

Table 4. Electrode Corrections for Granite

Frequency (Hz)	Long Cylinder		Small Disc		Electrode		Corrected Cylinder		Corrected Disc		$\rho = (R_S - R_e) \frac{A}{d}$	$\chi = (X_S - X_e) \frac{A}{d}$
	R <sub>S1</sub>	-X <sub>S1</sub>	R <sub>S2</sub>	-X <sub>S2</sub>	R <sub>e</sub>	-X <sub>e</sub>	R <sub>S1</sub> -R <sub>e</sub>	-(X <sub>S1</sub> -X <sub>e</sub> )	R <sub>S2</sub> -R <sub>e</sub>	-(X <sub>S2</sub> -X <sub>e</sub> )		
							$\rho$	$\chi$				
5.027	921.7	3152	248.6	483.9	225.3	391.8	696.4	2760	23.3	92.1	6.40	25.6
6.013	720.8	2755	205.8	430.5	188.0	350.3	522.8	2405	17.8	80.3	4.90	22.3
7.96	544.0	2280	152.2	353.5	138.7	287.0	405.3	1993	13.5	66.5	3.80	18.5
9.96	421.4	1775	119.5	297.5	109.1	246.5	312.3	1528.5	10.4	51.0	3.00	14.2
20.07	465.8	944.9	63.01	173.8	49.1	147.2	416.7	797.7	13.9	26.6	3.90	7.4
40.20	240.2	688.8	28.91	103.0	21.6	82.78	218.6	606	7.3	20.2	2.03	5.6
60.10	163.0	525.8	17.07	73.69	12.0	58.1	151.0	467.7	5.04	15.6	1.40	4.3
1000	1.172	31.71	1.503	5.65	---	4.7	---	26.96	---	0.9	---	0.3
2028	1.920	15.91	1.154	2.97	1.128	2.5	0.792	13.39	0.026	0.4	0.01	0.1

By subtracting the data in columns 6 and 7 point by point from the corresponding measured impedance data, and multiplying each resulting number into  $(A/d)$ , the basaltic specific resistance  $\rho$ , and reactance  $\chi$ , were calculated and recorded in columns 12 and 13 of Table 3.

A check on the validity of this technique was made by cutting a third section of the basalt sample with length 0.150 cm. Repeated measurements on this third sample gave data which agreed closely with those just reported. The specific impedance data for this third sample were calculated and found to be within the one percent error from those recorded in Table 3. This agreement supports our technique of correcting for the electrode impedance artifacts and lends credence to the validity of our impedance measurements.

From here on, each rock sample will be cut into two unequal lengths and the ratio  $\alpha$  of the two lengths will be accurately determined. The computer program will be modified to automatically correct for electrodes by Equations (19) and (20) before the final data of  $\rho$  and  $\chi$  will be displayed.

In a similar manner, the electrode corrections for granite were applied and the data in Table 4 were obtained. The plots of the specific reactance  $\chi$  against the specific resistance  $\rho$  at a series of frequencies for basalt, granite and quartzite are shown in Figure 10. The impedivity of each of these three rocks expressed in ohms  $\times$  meter is thus determined at frequencies between 1 and 2000 Hz.

#### H. TRANSFORMATION OF IMPEDANCE PARAMETERS TO DIELECTRIC PARAMETERS

An important phase of this research is to provide techniques for the extraction of the real and imaginary parts of the dielectric constant ( $\epsilon$ ) from their impedance counterparts, namely the imaginary and the real parts of the electric impedance,  $Z$ .

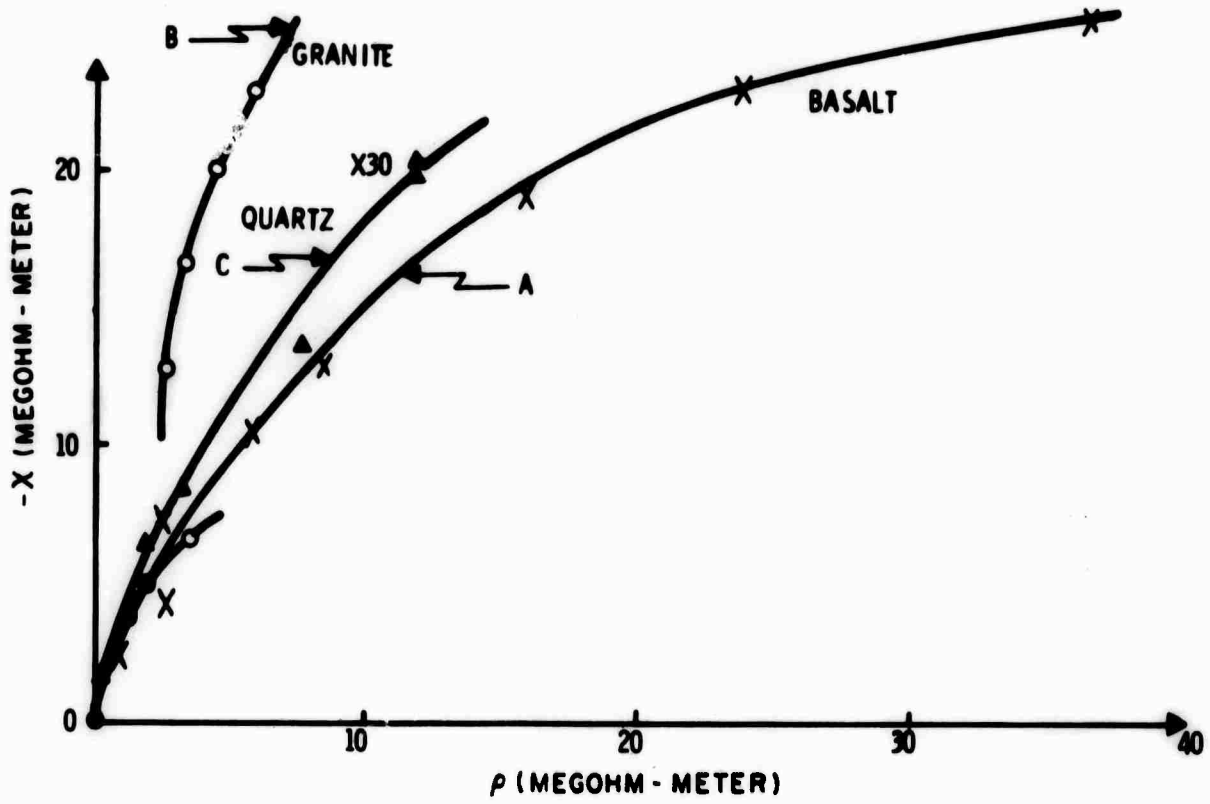


Figure 10. Specific Impedance Parameters for A - Basalt; B - Granite; and C - Quartzite

Thus,

$$\epsilon = \epsilon' - J\epsilon''$$

and

$$Z = R + JX$$

If the dielectric is symbolically represented by a simple R-C unit (see Appendix A), then the relation between X and R on the one hand, and  $\epsilon''$  and  $\epsilon'$  on the other hand establishes a full semicircle in the Argand diagram, and the Cole-Cole plot respectively. The circle will have its center on the real axis and will pass by the point of origin, i. e., the coordinates of the circle center will be (r, 0) where r is the circle radius. Since the conformal transformation ( $W - Z^{-1}$ ) of a circle results in a circle, a plot of the conductance G versus the susceptance  $\omega C$ , instead of X versus R, establishes a circular arc.

This study, has developed a model that simulates the dielectric dispersion of a real system (see Appendix B). An important criterion is that this model possesses a single time-constant or relaxation time, in contrast to previous investigators (References 7, 8, 9, and 10) who used a distribution of relaxation times to account for the dispersion in a real system that results in a circular arc with a depressed center in the Argand or the Cole-Cole diagram. In the following procedure, we are going to use the "bracketing" technique which relates the boundary points in both the dielectric and the impedance circular arcs, and to invoke the principle that the same relaxation process, with a characteristic time,  $\tau$ , is responsible for both the dielectric and the impedance arcs, i. e., we assume a constant relaxation time.

The relaxation time for a dielectric dispersion process following the Maxwell-Wagner mechanism, is related to the volume resistivity by the following equation (Reference 11):

$$\tau = \epsilon \epsilon_r \rho \quad (21)$$

where  $\epsilon_r$  is the permittivity of free space ( $8.85 \times 10^{-12}$  farad per meter) and  $\rho$  is the volume resistivity defined by

$$R = \rho \left(\frac{d}{A}\right) \text{ or } \rho = R \left(\frac{A}{d}\right) \quad (22)$$

where  $A$  is the rock sample cross-sectional area (electrode area) and  $d$  is the thickness of the rock specimen (the interelectrode distance).

At the two boundary points of infinite and zero frequency, respectively, the application of Equation (21), with the provision that the value of  $\epsilon$  decreases with increasing frequency, leads to

$$\tau = \epsilon_{\infty} \epsilon_r \rho_0 = \epsilon_{\infty} \epsilon_r R_0 \left(\frac{A}{d}\right) \quad (23)$$

and

$$\tau = \epsilon_0 \epsilon_r \rho_{\infty} = \epsilon_0 \epsilon_r R_{\infty} \left(\frac{A}{d}\right) \quad (24)$$

This is true because we like our model to be presented with a single relaxation time.

The dielectric constants at infinite and zero frequency can therefore be calculated from

$$\epsilon_r \epsilon_{\infty} = \left(\frac{\tau}{R_0}\right) \left(\frac{d}{A}\right) \quad (25)$$

and

$$\epsilon_r \epsilon_0 = \left(\frac{\tau}{R_{\infty}}\right) \left(\frac{d}{A}\right) \quad (26)$$

The relaxation time can be related to our model parameters (see Appendix B), in the following manner:

$$\tau = (R_0 - R_\infty) C_p \sqrt{1 + \cotan^2 \phi} \quad (27)$$

where  $\phi$  is the phase angle derived from the impedance diagram as follows:

$$\phi = \sin^{-1} \left[ \frac{R_0 - R_\infty}{2r} \right] \quad (28)$$

where  $r$  is the radius of the circle whose arc represents the Argand diagram.

The Cole-Cole parameter,  $\alpha$ , is related to the phase angle,  $\phi$ , as follows:

$$\phi = \frac{\pi}{2} (1 - \alpha) \quad (29)$$

In the ideal case of a Debye dielectric,  $\phi = \frac{\pi}{2}$  and  $\alpha = 0$ . In general,  $\alpha$  is a fraction, usually close to 0.5.

The capacitance,  $C_p$  needed in Equation 27 for calculating the relaxation time can be obtained from the impedance data as follows:

$$C_p = \frac{-X_\omega}{\omega(R_\omega - R_\infty)^2 + X_\omega^2} \quad (30)$$

Plotting  $C_p$  as a function of frequency, a sharp decrease occurs between 0.01 and 100 Hz, which is followed by a plateau between 100 Hz to 2,000 Hz. The average value of this plateau is considered to represent  $C_p$ .

Using the phenomenological equations of the complex dielectric constant (References 7, 12).

$$\epsilon = \epsilon_{\infty} + \frac{\epsilon_0 - \epsilon_{\infty}}{1 + (J\omega\tau)^{1-\alpha}} = \epsilon' - J\epsilon'' \quad (31)$$

Equation (31) is separable into its real and imaginary parts using the identity:

$$j^{\alpha} = e^{\frac{j\pi}{2} \alpha} \quad (32)$$

to give

$$\epsilon' = \epsilon_{\infty} + \frac{\epsilon_0 - \epsilon_{\infty}}{2} \left[ 1 - \frac{\sinh (1-\alpha) S}{\cosh (1-\alpha) S + \cos \left(\frac{\alpha\pi}{2}\right)} \right] \quad (33)$$

and

$$\epsilon'' = \frac{\frac{1}{2} (\epsilon_0 - \epsilon_{\infty}) \cos \left(\frac{\alpha\pi}{2}\right)}{\cosh (1-\alpha) S + \sin \left(\frac{\alpha\pi}{2}\right)} \quad (34)$$

where S is given by

$$S = \log_e (\omega\tau) \quad (35)$$

The plot of  $\epsilon''(\omega)$  as a function of  $\epsilon'(\omega)$  as calculated from Equations (33) and (34) gives the Cole-Cole diagram.

The necessary operational steps in accordance with the foregoing equations were, therefore, added to the computer algorithm to extract the dielectric permittivity data from the specific impedance parameters. Provision for correcting the measured impedance parameters for electrode effects were also included in the program. The following subsection summarizes the dielectric data obtained with this procedure.

## I. COLE-COLE DIAGRAMS - DIELECTRIC AND IMPEDANCE PARAMETERS OF DRESSER BASALT

Basaltic sample (III) was obtained in the form of a cylinder with diameter 2.17 cm. Thin slices that measured 0.30 and 0.61 cm in length were cut from this sample. The ratio ( $\frac{A}{d}$ ) for the thinner slice was 0.1232 meter and for the thicker slice was 0.0618 meter. The electrode impedances were calculated with the aid of Equations (19) and (20) for the two slices. The electrode impedances were subtracted point by point from the corresponding measured impedance values. The resulting data were then multiplied into ( $A/d$ ) to give the specific resistance and reactance of basalt. Photostatic copies of the computer output for the two basaltic slices are shown in Tables 5 and 6.

Dielectric permittivity at each frequency was calculated from the model parameters as described in subsection H. The Cole-Cole plots resulting from these data are shown in Figures 11 and 13 for the 0.30 and 0.61 cm slices of basalt, respectively. These figures can be considered to be in satisfactory agreement within experimental error. The dielectric dispersion curves for basalt are shown in Figures 12 and 14 for the 0.30 and 0.61 cm slices of basalt. The relaxation times calculated from either the maximum in dielectric loss,  $\epsilon''$ , or the inflection point in the  $\epsilon'$  curve were found to be 16.6 and 13.4 milliseconds for the two basalt slices. Since the experimental measurements on both slices were completely independent of each other, the derived values of relaxation time are considered to be in reasonable agreement.

Table 7 summarizes the impedance and dielectric permittivity data on the two basalt slices. The dc resistivity of basalt,  $\rho_o$ , is estimated as  $1.27 \times 10^8$  and  $1.00 \times 10^8$  ohm meter for the thin and thick slices, respectively. These resistivity data appear to be internally consistent with each other and are in agreement with the value  $1.26 \times 10^8$  ohm meter reported in Parkhomenko (Reference 13) for dry basalt. The agreement is surprising in view of the anticipated differences between our Dresser basalt and Parkhomenko's most

Table 5. Impedance and Dielectric Data on Basalt (III)

ENTER NS,AOD PUT SSW1 UP FOR ELECTRODE CORRECTION  
#69.12317

K4-1 7/2/71		AOD= #.12317 PHASE AND AMPLITUDE CORRECTED					
FRQ	RS	XS	PAOD	XAOD	PHI	Z	
#.#99	931.#156	-122.4131	114.6732	-15.#776	-7.491#	939.#288	
#.15#	433.#498	-197.616#	53.3387	-24.34#4	-24.53#7	476.##06	
#.2#1	376.8926	-214.26#1	46.4219	-26.39#4	-29.62#1	433.5383	
#.4#3	3#7.59#6	-275.5842	37.8859	-33.9437	-41.8617	412.9874	
#.6#1	227.#444	-224.#116	27.9651	-27.5915	-44.6181	318.952#	
#.8#1	267.1763	-255.4711	32.9#81	-31.4664	-43.72#3	369.66#2	
1.##2	236.5#63	-21#.#7373	29.13#5	-25.9565	-41.7#55	316.7735	
2.#12	151.						
	.219	-169.7444	18.6#14	-2#.#9#74	-48.344#	227.2#2#	
4.#22	89.2898	-12#.#6417	1#.#9978	-14.8594	-53.4979	15#.#9#3	
6.##9	66.2687	-99.155#	8.1623	-12.2129	-56.248#	119.2613	
1#.#52	41.1296	-67.223#	5.#659	-#.#2799	-58.5444	78.8#73	
2#.#72	28.#718	-41.7#85	3.4576	-#.#1372	-56.#617	5#.#2755	
6#.#96	1#.#7#81	-23.1228	1.3189	-2.848#	-65.1561	25.4819	
1#.#6#4	7.#6#2	-17.3957	#.#8696	-2.1426	-67.9147	18.7739	
2#1.342	3.4155	-1#.##66#	#.				
			2#7	-1.2398	-71.2624	1#.#6297	
6#3.448	1.3968	-3.7563	#.172#	-#.#4627	-69.6#79	4.##76	
1#99.174	1.1544	-2.2427	#.1422	-#.#2762	-62.7682	2.5223	
15#9.434	1.#485	-1.561#	#.1291	-#.#1923	-56.1152	1.88#4	
2#25.783	#.9#39	-1.1397	#.1113	-#.#14#4	-51.585#	1.4546	

RS, XS CIRCLE FIT RESULTS- CIRCLE CENTER = 511.1931 37#.#758#  
RADIUS = 638.4723  
FIT = 3.4752

R# = 1#3#.#9866 RINF = -8.6#55

MODEL PARAMETERS - R1 = 1545.4873/FRQ  
RP = 1#39.5872  
CP = #.17#1E-#3

CP = #.13#332E-#4

TAU = 16.6#434#SEC E# = 1771.1357 E1NF = 14.77477

FRQ	EP	EPP
#.#99	-#.#168186E #4	-#.#851248E #2
#.15#	-#.#1657#1E #4	-#.#1#664#E #3
#.2#1	-#.#1637#3E #4	-#.#124742E #3
#.4#3	-#.#157142E #4	-#.#178948E #3
#.6#1	-#.#152152E #4	-#.#217142E #3
#.8#1	-#.#147941E #4	-#.#247313E #3
1.##2	-#.#144257E #4	-#.#272144E #3
2.#12	-#.#13#321E #4	-#.#3526#4E #3
4.#22	-#.#112952E #4	-#.#422121E #3
6.##9	-#.#1#1618E #4	-#.#448484E #3
1#.#52	-#.#864#7E #3	-#.#459785E #3
2#.#72	-#.#662553E #3	-#.#432#68E #3
6#.#96	-#.#393816E #3	-#.#32#979E #3
1#.#6#4	-#.#298125E #3	-#.#261763E #3
2#1.342	-#.#199427E #3	-#.#19#3#6E #3
6#3.448	-#.#994948E #2	-#.#1#7468E #3
1#99.174	-#.#697422E #2	-#.#8#7933E #2
15#9.434	-#.#518329E #2	-#.#642934E #2
2#25.783	-#.#411467E #2	-#.#542893E #2

\*\*\*\*\* STOP \*\*\*\*\*

Table 6. Impedance and Dielectric Data on Basalt (III).  
0.61 cm slice.

MORE  
DONE

ENTER NS, AOD PUT SSW1  $\text{UP}$  FOR ELECTRODE CORRECTION  
#68. #6184

K2-1 7/2/71		AOD= #.6184		PHASE AND AMPLITUDE CORRECTED		
FRQ	RS	XS	RAOD	XAOD	PHI	Z
.099	14.6372	-292.5101	86.6166	-18.0765	-11.7890	1450.8542
.201	630.5455	-296.0410	58.9804	-18.5072	-23.1590	696.3999
.402	531.9665	-568.3069	52.8968	-22.7761	-54.6994	647.0226
.602	532.7693	-412.9792	32.9464	-25.5586	-57.7840	674.0804
.801	459.8779	-345.4170	27.2020	-21.2569	-57.9823	588.0371
1.003	342.4744	-532.4679	33.5466	-54.1646	-43.3262	774.2753
2.008	518.4326	-425.5148	19.6951	-26.1902	-53.0654	329.8858
4.023	184.9092	-297.8154	11.4548	-18.4169	-58.1687	550.5502
6.010	130.7422	-228.6871	8.0851	-14.1420	-60.24; 5	265.4224
7.999	90.7913	-172.8300	5.6145	-10.6878	-62.2906	193.2262
10.026	80.4771	-131.9040	4.9767	-9.5957	-62.0904	171.9052
20.048	34.3092	-88.4668	5.5708	-5.4708	-58.3648	103.9116
60.096	20.5684	-46.3154	1.2719	-2.8641	-66.0591	50.6771
100.200	14.1226	-33.6855	0.8753	-2.2067	-68.4127	58.5766
200.555	5.9685	-19.9417	0.3691	-1.2532	-75.5451	20.8157
605.448	2.4719	-7.3750	0.1529	-0.4561	-71.4755	7.7703
1009.174	2.0572	-4.4140	0.1260	-0.2730	-65.2302	4.8614
1312.200	1.9527	-3.0350	0.1200	-0.1877	-57.2467	5.6089
2023.785	1.8239	-2.1429	0.1129	-0.1325	-49.5692	2.8135

RS, XS CIRCLE FIT RESULTS- CIRCLE CENTER = 817.1544 512.9148  
RADIUS = 970.6765  
FIT = 0.4203

R# = 1650.6567 RINF = -16.5679

MODEL PARAMETERS - R1 = 4016.5664/FRQ  
RP = 1667.0046  
CP = 0.8316E-04

CP = 0.685079E-03

TAU = 15.40942MSEC E# = 1496.9577 EINF = 14.84582

FRQ	EP	FPP
.099	-0.144029E 04	-0.553130E 02
.201	-0.140918E 04	-0.845058E 02
.402	-0.136220E 04	-0.126864E 03
.602	-0.132322E 04	-0.158669E 03
.801	-0.129566E 04	-0.184666E 03
1.003	-0.126515E 04	-0.207210E 03
2.008	-0.115659E 04	-0.284185E 03
4.023	-0.101591E 04	-0.361508E 03

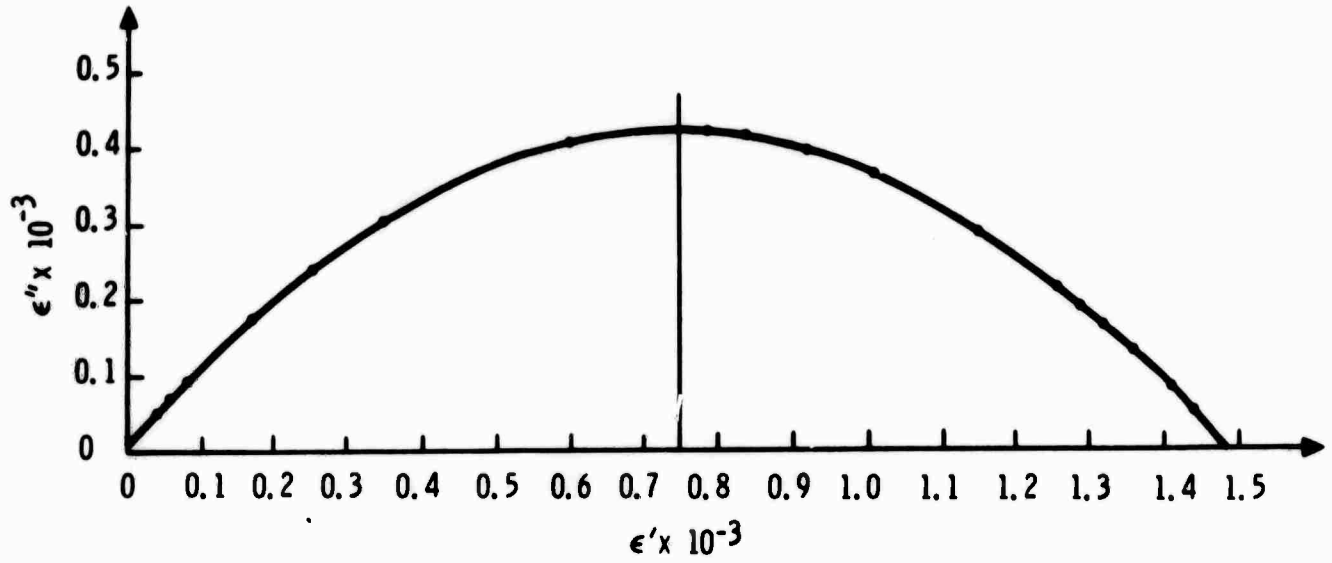


Figure 11. Cole-Cole Plot of Dresser Basalt. Data on 0.61 cm slice.

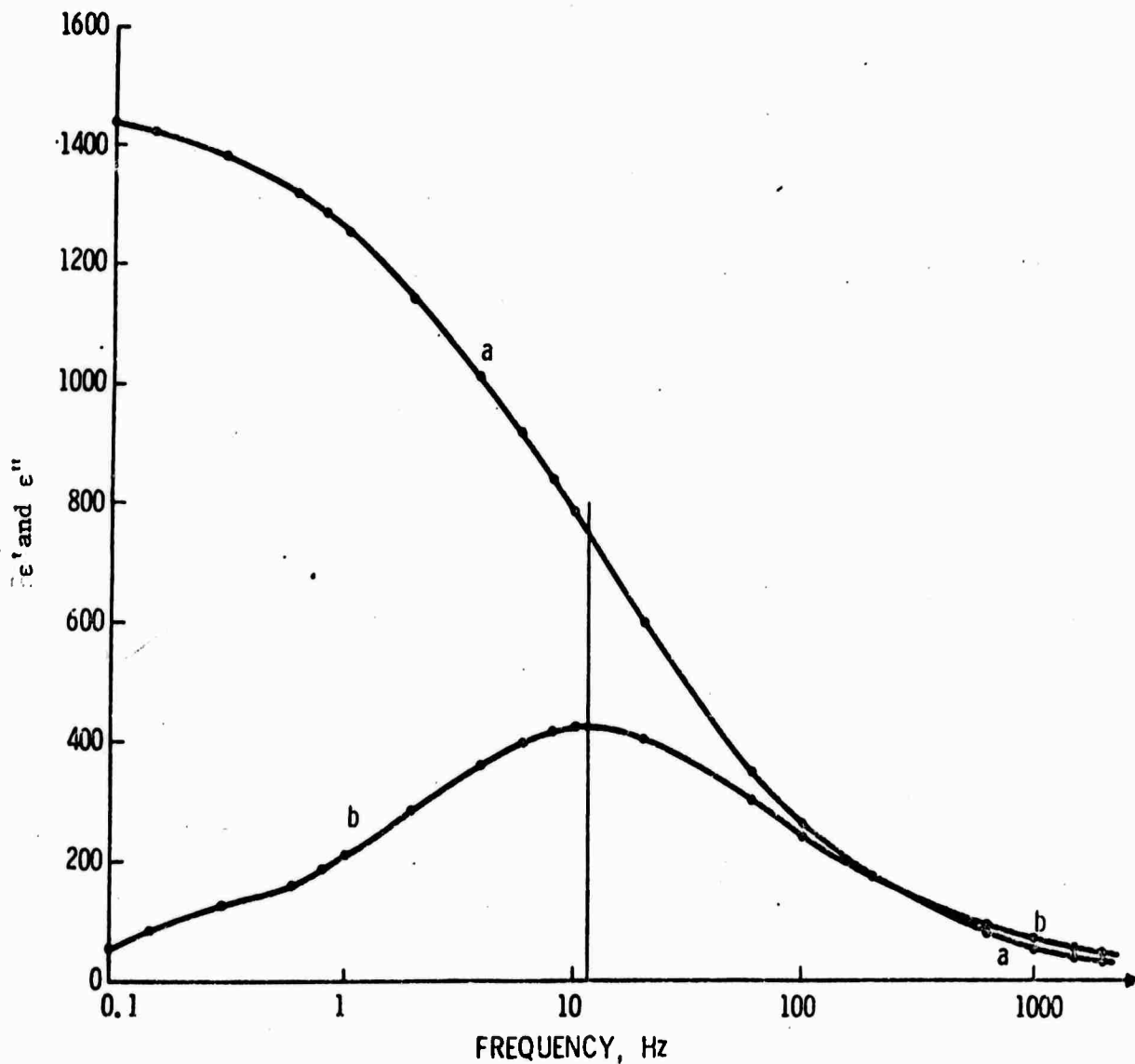


Figure 12. Dielectric Permittivity of Dresser Basalt as a Function of Frequency (a - Real Part of Dielectric Constant,  $\epsilon'$ ; b - Imaginary Part,  $\epsilon''$ ). Data on the 0.61 cm slice; relaxation time,  $\tau = 13.4$  millisecond.

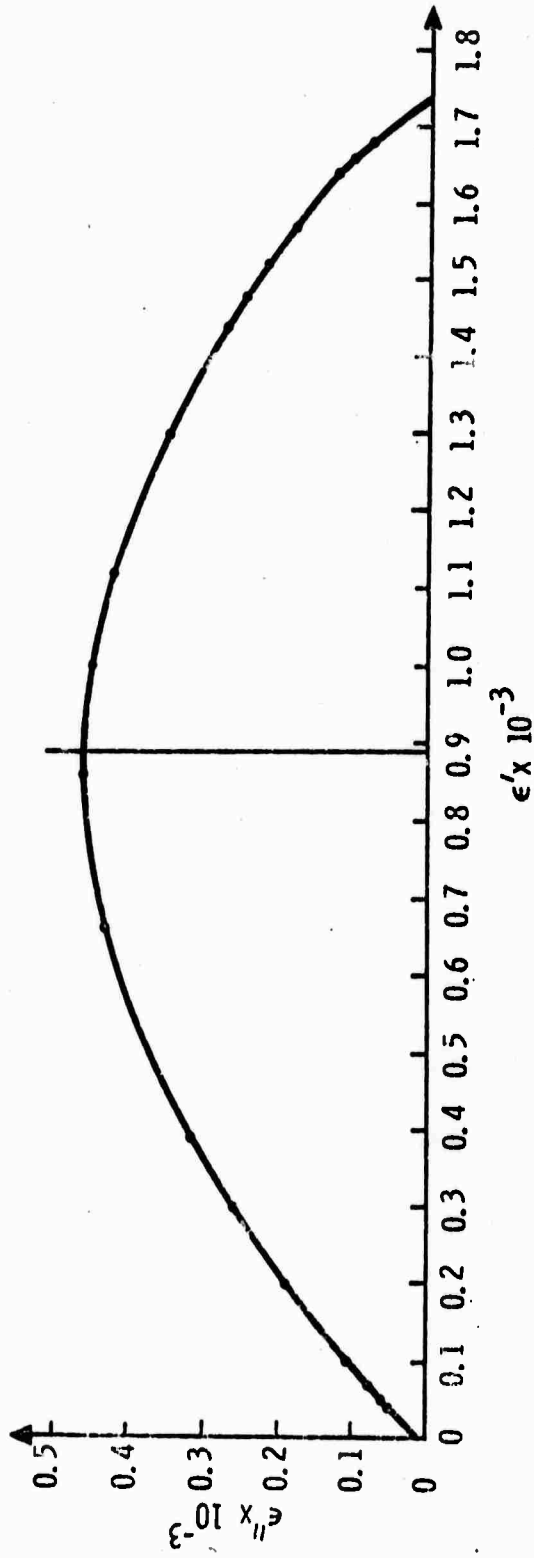


Figure 13. Cole-Cole Plot of Dresser Basalt. Data on 0.30 cm slice.

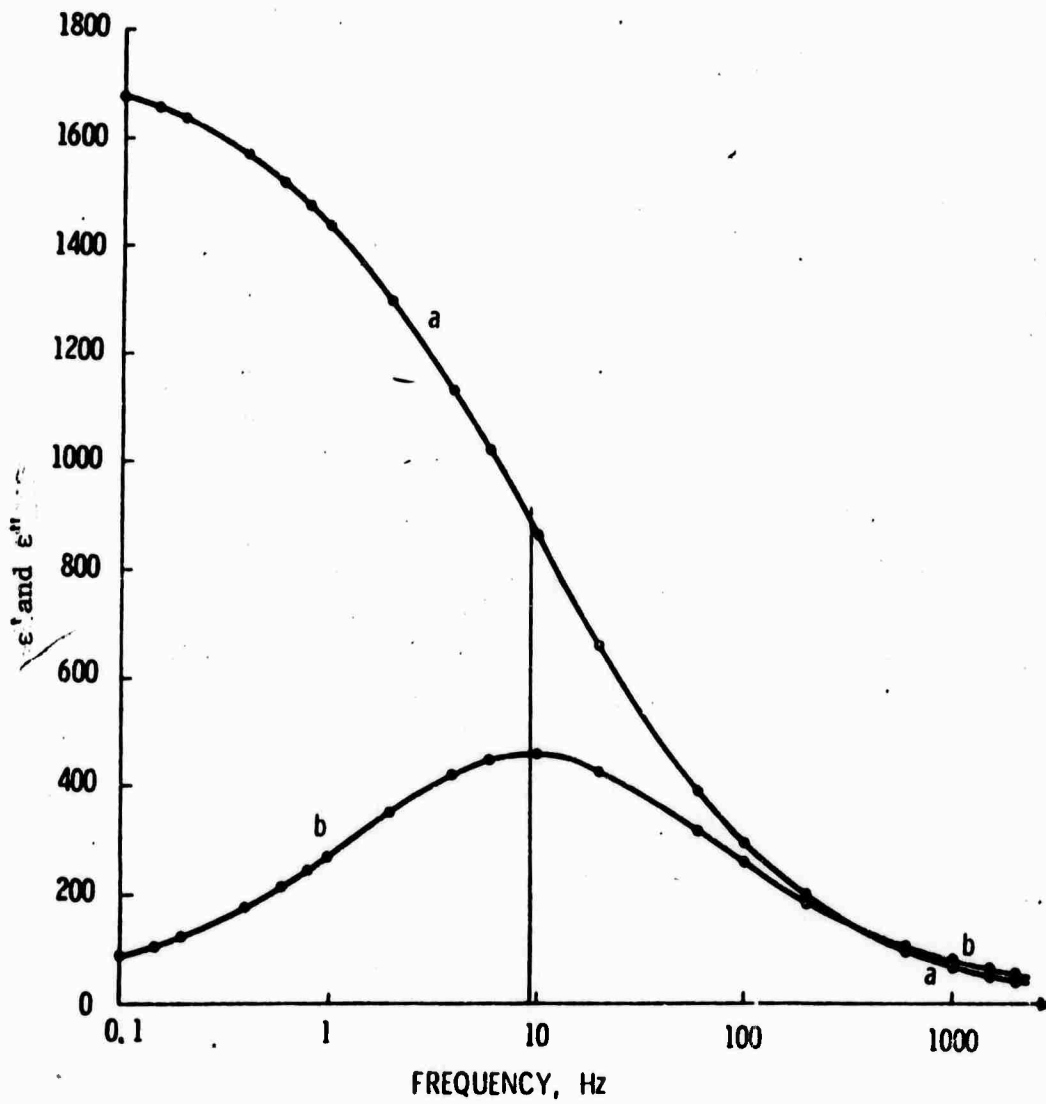


Figure 14. Dielectric Permittivity of Dresser Basalt as a Function of Frequency (a - Real Part of Dielectric Constant,  $\epsilon'$ ; b - Imaginary Part,  $\epsilon''$ ). Data on the 0.30 cm slice; relaxation time,  $\tau = 16.6$  milliseconds.

Table 7. Electric and Dielectric Parameters of Dresser Basalt

Parameter	0.30 cm Slice	0.61 cm Slice
dc resistivity, $\rho_0$ , ohm meter	$1.27 \times 10^8$	$1.00 \times 10^8$
infinite frequency resistivity, $\rho_\infty$ , ohm meter	$1.06 \times 10^6$	$1.01 \times 10^6$
model parallel resistance, $R_p$ , ohm	$8.89 \times 10^{14}$	$6.87 \times 10^{14}$
model capacitance, $C_p$ , farad	$1.3 \times 10^{-5}$	$6.8 \times 10^{-6}$
relaxation time, $\tau$ , second	$16.6 \times 10^{-3}$	$13.4 \times 10^{-3}$
zero frequency dielectric constant, $\epsilon_0$	$1.77 \times 10^3$	$1.50 \times 10^3$
infinite frequency dielectric constant, $\epsilon_\infty$	14.8	14.8
maximum dielectric loss, $\epsilon_{\max}$	$4.6 \times 10^2$	$4.2 \times 10^2$
$\rho_0 \epsilon_\infty' \epsilon_r$ , second	$16.4 \times 10^{-3}$	$13.1 \times 10^{-3}$
$\rho_\infty \epsilon_0' \epsilon_r$ , second	$16.6 \times 10^{-3}$	$13.2 \times 10^{-3}$

probably Russian basalt (origin not given). Table 7 also shows that the zero frequency dielectric constant of basalt is  $1.77 \times 10^3$  and  $1.50 \times 10^3$  for the thin and thick slices. The internal agreement in this case is also acceptable. Parkhomenko (Reference 14) reports that at low frequencies,  $10^2$  to  $10^4$  Hz, the dielectric constant assumes very large values ( $10^3$  to  $10^5$ ).

Keller (Reference 15) observed that the product of the dielectric constant at low frequency,  $\epsilon_0$ , into the resistivity at low frequency,  $\rho_0$ , is nearly a constant characteristic of a particular type of rock. For rhyolite and basalt, the average value of  $\rho_0 \epsilon_0$  is 0.63 sec with the range of 19 values from 0.25 to 26 sec. Average values of this product varied from  $1.4 \times 10^{-3}$  for basic igneous rocks such as gabbro and chromite to 10.8 for the hematite ore from Minnesota, which contains appreciable quantities of electronically conducting materials. The data in Table 7 also show that the products  $\rho_0 \epsilon_\infty \epsilon_r$  and  $\rho_\infty \epsilon_0 \epsilon_r$  are equal to the relaxation time for both the thin and thick samples of basalt.

Similar experiments to those described above were run on a cylindrical quartzite sample of 2.22 cm diameter, 0.955 cm in length and an  $(\frac{A}{d})$  ratio of 0.0496 meter. The computer output data on this sample are shown in Table 8. From the present data, one can calculate the d-c resistivity of quartzite,  $\rho_0$ , from the observed value  $R_0$  of 31737.0 Megohm, thus

$$\rho_0 = R_0 \left(\frac{A}{d}\right) = 3.17 \times 0.041 \times 10^{10} = 1.29 \times 10^9 \text{ ohm-meter}$$

The relaxation time of this quartzite sample is also calculated to be 60.3 milliseconds. The real component of the dielectric constant at infinite frequency,  $\epsilon'_\infty$ , is determined as 5.29. Also, the real component of the quartzite dielectric constant at the limit of zero frequency,  $\epsilon'_0$ , is found to be  $3.95 \times 10^3$ .

Further trials are currently in progress to improve the model used to derive the rock electrical parameters and the steps by which impedance data are transformed to dielectric data.

Table 8. Impedance and Dielectric Data on Quartzite  
0.30 cm slice.

ENTER NS,AOD PUT SSW1 UP FOR ELECTRODE CORRECTION  
076.04062

N3 08/26/71			AOD= 0.04062		PHASE AND AMPLITUDE CORRECTED		
FRQ	RS	XS	RAOD	XAOD	PHI	Z	
1.001	906.0527	-4305.7520	36.8039	-174.8996	-78.1225	4400.0498	
2.004	858.0356	-3565.0869	34.8534	-144.8138	-76.4732	3666.8282	
4.008	473.6096	-1959.4707	19.2380	-79.5937	-76.4177	2015.8948	
6.017	329.4869	-1296.3813	13.3838	-52.6590	-75.7453	1337.5972	
8.026	299.3496	-1046.7861	12.1596	-42.5205	-74.0465	1088.7478	
10.038	285.1741	-825.8511	11.5838	-33.5461	-70.9549	873.7014	
20.153	294.2329	-513.6184	11.9517	-20.8632	-60.1976	591.9265	
40.161	137.3826	-395.5394	5.5805	-16.0668	-70.8516	418.7188	
60.168	26.0035	-291.0387	1.0595	-11.0220	-84.8850	292.2051	
79.872	-43.7361	-229.9436	-1.7766	-9.3403	-100.7766	234.0660	
99.800	-32.5157	-183.0712	-1.3208	-7.4364	-100.0787	185.9364	
201.884	-14.8700	-75.4577	-0.6041	-3.0651	-101.1562	76.9091	
504.202	-2.9886	-24.6946	-0.1214	-1.0031	-96.9075	24.8743	
998.185	0.6537	-11.1146	0.0265	-0.4515	-86.6404	11.1338	
1506.591	1.7666	-7.0809	0.0717	-0.2076	-75.9968	7.2979	
2022.059	2.0117	-5.2798	0.0817	-0.2145	-69.1470	5.6501	
2537.594	1.2796	-4.3307	0.0519	-0.1759	-73.5441	4.5158	

RS, XS CIRCLE FIT RESULTS- CIRCLE CENTER = 15890.1699 1622.5833  
RADIUS = 15930.5625  
FIT = 0.6057

R0 = 31737.8828 RINF = 42.4551  
MODEL PARAMETERS - R1 = 268343.750/FRQ  
RP = 31695.4258  
CP = 0.9060E-05

CP = 0.189275E-05

TAU = 60.30515MSEC E0 = 3951.31494 EINF = 5.28559

FRQ	EP	EPP
1.001	0.281805E 04	0.127285E 04
2.004	0.223135E 04	0.172910E 04
4.008	0.159191E 04	0.166165E 04
6.017	0.125202E 04	0.136837E 04
8.026	0.103396E 04	0.115927E 04
10.038	0.804613E 03	0.989095E 03
20.153	0.516610E 03	0.557240E 03
40.161	0.291078E 03	0.301209E 03
60.168	0.205644E 03	0.208085E 03
79.872	0.160041E 03	0.160254E 03
99.800	0.132528E 03	0.130402E 03
201.884	0.721628E 02	0.677588E 02
504.202	0.339802E 02	0.288582E 02
998.185	0.204895E 02	0.152495E 02
1506.591	0.156443E 02	0.103800E 02
2022.059	0.131570E 02	0.788417E 01
2537.594	0.116534E 02	0.637630E 01

\*\*\*\*\* STOP \*\*\*\*\*

SECTION IV  
TECHNICAL REPORT SUMMARY

The research program described in this report was initiated six months ago at Honeywell Systems & Research Division with the objective of applying dielectric relaxation theories to rocks, and to utilize the dielectric parameters and the closely-related electrical impedance parameters to obtain significant correlates with rock geophysical characteristics and ultimate structure. The information gathered will be pertinent to rock fragmentation, excavation and underground tunnelling problems. The degree of attenuation of magnetic fields from a flat-lying loop in an underground tunnel depends on the electrical resistivity of the overlying rock and hence electromagnetic communication with underground tunnels and mines will be greatly improved from an accurate knowledge of rock impedance and dielectric properties. The data gathered will also be relevant to the presence of underground water, entrapped water and gases in rocks, and similar factors needed ahead of excavation and underground tunnelling. To achieve these goals, accurate and rapid methods of displaying rock electrical impedance (both resistive and reactive) and dielectric permittivity, will first be developed.

Our present novel techniques of impedance data display permits direct evaluation of the dc resistance,  $R_0$  (which is directly related to dielectric permittivity at zero frequency,  $\epsilon_0$ ); the resistance at infinite frequency (which is directly related to the permittivity  $\epsilon_\infty$ ); and the impedance (and complex dielectric constant) at any frequency in between. Hence, as a first step, our existing impedance equipment with its on-line computer capabilities was modified to measure the complex impedance of rocks. A brief description of the new equipment is given in Section II of this report. It is highly desirable to extend the capability of this equipment (beyond the kilohertz frequency range). Extension to the mega- and gigahertz range has been

recommended in Honeywell proposal 1D-E-3, "Effect of Frequency and Temperature on Rock Dielectric Parameters", which was recently submitted to the contracting agency.

The complex impedance of rock samples at a range of frequencies that brackets their turnover frequency would yield valuable information on the relaxation time(s) of the silica tetrahedra and other structural groups within the rock, and the presence or absence of conductive minerals. In general, a Cole-Cole (Reference 7) circular-arc plot would be obtained in the complex dielectric diagram. With complex structures, the resulting figure may be analyzed into a series of nearby semicircular arcs, each describing a given relaxation mechanism with some interaction coefficients among the various aggregates. The same Cole-Cole plot can be obtained in a complex impedance diagram, sometimes called Argand diagram. Sinbel (Khalafalla, Reference 16) showed that the plot of the series reactance,  $X_s$ , against the series resistance,  $R_s$  (both determined at a given frequency), in a complex system should yield a semicircular arc. The intersection of this circular arc with the real (resistive) axis will define the dc resistance,  $R_0$  (at the farthest right end). Any point on the arc will define the impedance radius vector with both its reactive and resistive components. The results shown in Figures 1, 2, 3 and 5 in Section I, and 7, 8, 11 and 13 in Section III amply support the validity of our concepts. Impedance data were gathered on basalt, granite and quartzite, and despite the wide variation in electrical properties of these rocks, we were able to fit their data to appropriate circular arcs.

Relaxation-times and rock characteristic frequencies can be easily determined by displaying the  $X_s$  data and  $R_s$  data as functions of frequency in semilogarithmic graphs. Theory indicates that  $X_s$  (and also the imaginary part of dielectric permittivity,  $\epsilon''$ , or the dielectric loss) exhibit a maximum value at the turnover or characteristic frequency. On the other hand, the resistive component of the impedance,  $R_s$  (and also the real part,  $\epsilon'$ , of

the complex dielectric permittivity) will undergo a sudden dispersion at the turnover frequency. Our experimental data shown in Figures 6, 8, 9, 12 and 14 in Section III are in full agreement with these predictions. The application of these fundamental impedance and dielectric theories to rocks is rather novel, and is only possible because of the accuracy and rapidity of our technique of data acquisition.

Electrode polarization effects are always encountered in electrical measurements of complex systems. A method is developed in Section III, subsection C to correct for electrode polarization by cutting thinner slices of the same rock. The method was applied with success on the impedance data of basalt and granite. The electrode effects are significant for thin rock samples where they may constitute a substantial segment of the measured impedance. While the electrode corrections may be neglected for longer rock samples, sometimes impedance measurement may be exceptionally difficult because of amplifier saturation at the very high impedance levels. It is concluded that, whenever possible, electrode polarization effects should be determined, and corrected for, by repeating the impedance measurement on a thin slice of the same rock sample.

The effect of temperature and pressure on relaxation time and characteristic frequency can be used to calculate the activation energy, activation entropy, and activation volume of the aggregate interactions. This new set of data can yield further information on the ultimate structure and petrogenesis of rocks.

These new areas of endeavor constitute the Honeywell long-range research goals and were submitted in a new proposal 1D-E-3 to the contracting agency. To validate the concepts presented in this proposal, we performed some preliminary measurements on basalt at two temperatures. The results, given in Section III, subsection G, of this report, indicate a significant temperature effect on both the relaxation time and the dc resistance of basalt. An

activation energy of about 0.5 ev for the relaxation of structural units within basalt was estimated. Further work on this interesting temperature effect will hopefully be conducted in the second phase of the project; i. e., in the following year.

A new technique was developed for the extraction of the dielectric parameters from the measured impedance parameters after electrode correction and size normalization was adopted. The method depends on "bracketting" the circular arc in both the Argand and the Cole-Cole plots and on the assumption that the single relaxation time must be the same for both. The computer algorithm has been extended to derive the dielectric loss,  $\epsilon''$ , and the real part of dielectric constant,  $\epsilon'$ , at various frequencies from the measured specific impedance parameters. The results on basalt agree reasonably well with those reported in literature and are described in Subsections H and I of Section III.

Research efforts in the following six months will be devoted to developing and improving the electrical models that are capable of simulating the complex impedance of rocks, and to apply these models to the gathered data. Further emphasis will be placed on investigating the effects of rock size, rock shape and dimensions, as well as degree of dryness and humidity on the generated impedance data.

SECTION V  
LITERATURE CITED

- 1) Khalafalla, A. S., L. Turner and D. Spyker, "An Electrical Model to Simulate Skin Dielectric Dispersion," presented at the 5th Annual Meeting of the Association for the Advancement of Medical Instrumentation, Boston, March 1970 (In Press, July 1971 issue of computers in Biomedical Research.
- 2) Lindroth, D. P., and Krawza, W. G., "Heat Content and Specific Heat of Six Rock Types at Temperatures up to 1000°C," Bureau of Mines Report of Investigation No. 7503, April 1971.
- 3) Huggins, R. A., and Huggins, M. L., "Structural Defect Equilibria in Vitreous Silica and Dilute Silicates," *Journal of Solid-State Chemistry*, Vol. 2 (1970), pp. 385-395.
- 4) Information on this rock sample was provided orally by Mr. Carl Wingquist, Twin Cities Mining Research Center, U. S. Bureau of Mines.
- 5) Glasstone, S. K., J. Laidler and H. Eyring; "The Theory of Rate Processes," McGraw-Hill, New York (1951).
- 6) Takashima, S., and Schwan, H. P., "Dielectric Dispersion of Crystalline Powders of Amino Acids, Peptides, and Proteins," *J. Phys. Chem.*, Vol. 70 (1966), pp. 4176-82.
- 7) Cole, K. S., and R. H. Cole; "Dispersion and Absorption in Dielectrics. I. Alternating Current Fields," *J. Chem Physics*, Vol. 9 (1941), p. 341.
- 8) Wagner, K. W., "Erklärung der dielektrischen Nachwirkungsvorgänge auf Grund Maxwellscher Vorstellungen." *Arch. Electrotech.* 2, 371 (1914).
- 9) Yager, W. A., "Distribution of Relaxation Times in Typical Dielectrics." *Physics* 7, 434 (1936).
- 10) Kirkwood, J., and R. Fuoss, "Anomalous Dispersion and Dielectric Loss in Polar Polymers." *J. Chem Phys.*, 9, 329 (1941).
- 11) Daniel, Vera V., "Dielectric Relaxation," Academic Press, London (1967) p. 212.
- 12) Ibid, p. 97.

- 13) Parkhomenko, E. I., "Electrical Properties of Rocks." Translated from Russian and Edited by G. V. Keller, Plenum Press, New York (1967), p. 122.
- 14) Ibid, p. 224.
- 15) Keller, G. V., "Analysis of Some Electrical Transient Measurements on Igneous, Metamorphic and Sedimentary Rocks." Chapter in "Overvoltage Research and Geophysical Applications," Pergamon Press, London (1959), pp. 92-111.
- 16) Sinbel, A. (Khalafalla); "In-Vivo and In-Vitro Measurement of the Impedance and Phase Characteristics of Human Tissues by Mutual-Impedance Methods," Ph.D. Dissertation, University of Minnesota, (1966), pp. 229.

APPENDIX A  
ELECTRICAL MODELS TO SIMILATE ROCK IMPEDANCE

Impedance data at various frequencies usually describe a circular-arc plot when displayed in a cartesian diagram with the series reactance as ordinate and the series resistance as abscissa. The display is never a full semi-circle, but is a part of a circle whose center does not lie on the real axis (resistance), and is substantially below it. The phase angle is defined as half of the angle, subtended by the circular-arc at the center of the circle, i. e., between the two radii of the circle defining the two points of intersection of the arc with the resistive axis. An ideal dielectric dispersion model system is easily simulated by a parallel R-C unit, and can be shown to give a full semi-circular plot upon transformation to an iso-impedic series R-C unit.

A major objective of this research is to seek for correlations between one or more of the rock impedance parameters and its geophysical, structural, as well as genetic characteristics. If significant correlations are discovered, then the former parameters can be taken as a quantitative predictor of the latter measures. As a first step to achieve this goal, an adequate model capable of simulating the rock impedance data should be developed. This constitutes an important topic of the proposed investigation.

Sinbel (Khalafalla) (Reference 16) derived various analytical proofs of the semicircular arc in an attempt to describe the relationship of the equivalent series reactance to the corresponding resistance. The derivations were based on a parallel-to-series transformation of electrical models with a single time-constant. In the simplest case, it was shown that the transformation from a parallel R-C unit (with frequency independent components) to an adjustable series R-C unit (with the same total impedance) results in a full semicircular-arc plot in the Argand diagram. The locus of the series

reactance,  $X_s$ , when plotted against the series resistance,  $R_s$ , follows the analytical equation of a circle of radius,  $\frac{1}{2} R_p$ , where  $R_p$  is the parallel resistance assumed to be a constant quantity characteristic of the system, thus

$$X_s^2 + [R_s - \frac{1}{2} R_p]^2 = \frac{1}{4} R_p^2 \quad (A1)$$

The center of the semicircular plot should then have the coordinates  $(0, \frac{1}{2} R_p)$  and hence is located on the real or resistive axis. This seems to represent a very idealized situation. In real systems the semicircular arc observed experimentally is usually translated vertically downwards so that its center has the coordinates  $a$  and  $-b$ , and accordingly follows an equation of the form

$$[X_s + b]^2 + [R_s - a]^2 = c \quad (A2)$$

where  $a$ ,  $b$  and  $c$  are constants related to  $X_p$  and  $C_p$ .

The assumption of a leaky condenser was made by connecting a small resistance,  $r$ , to the parallel capacitor,  $C_p$ , in the idealized parallel R-C model. This resulted in relationships between  $X_s$  and  $R_s$  of the form

$$X_s^2 + \left[ R_s - \frac{R_p}{r + R_p} \left( r + \frac{1}{2} R_p \right) \right]^2 = \frac{R_p^4}{4(r + R_p)^2} \quad (A3)$$

This again represents an equation of a circle whose center lies on the real axis at a distance of  $R_p (r + \frac{1}{2} R_p) / (r + R_p)$  from the origin and whose radius is given by  $\frac{1}{2} R_p / (r + R_p)$ .

Several other alternatives were tried (Reference 16) by attaching resistors and capacitors to the fundamental  $R_p - C_p$  unit at various places. However, the ensuing circular arc plot did not in any case possess the limiting and boundary values expected from the electrical model. The developed

mathematical equations were unable to show, for example, that the circular arc plot would intercept the real axis at points corresponding to  $r$  and  $(r + R_p)$  as would be expected at the limits of infinite and zero frequencies, respectively. The futility was evident of describing a complex system by an electrical analog with conventional frequency independent components and a single time-constant.

A distribution of relaxation times can in principle yield expressions [of which Equation (31) in Section II is a special case] that are capable of explaining the observed results. This distribution is simulated by an infinite series of parallel R-C units with various time-constants. Unlike electrical models with a single time-constant, these mathematical simulations will probably fail to provide a one-to-one correspondence between the rock impedance parameters and its geophysical characteristics.

APPENDIX B  
ELECTRICAL ANALOG WITH ONE FREQUENCY  
DEPENDENT RESISTANCE

An electrical model, Figure B1 in which a frequency dependent resistance,  $r_1$ , is shunted across the condenser,  $C_p$ , is capable of describing a circular arc in the series domain with a vertically displaced center (Figure B2). A condition to be imposed on the resistor,  $r_1$ , is that its value changes inversely with the frequency such that  $r_1 = \frac{g}{f}$ , where  $g$  is a constant and  $f$  is the frequency. The total impedance of this model is given by

$$\begin{aligned}
 Z_p &= \frac{R_p \frac{jr_1 X_p}{r_1 + jX_p}}{\frac{jr_1 X_p}{R_p + r_1 + jX_p}} + r_2 \\
 &= \frac{r_1 R_p X_p^2 (r_1 + R_p)}{r_1^2 R_p^2 + X_p^2 (r_1 + R_p)^2} + j \frac{r_1^2 R_p^2 X_p}{r_1^2 R_p^2 + X_p^2 (r_1 + R_p)^2} + r_2 \quad (B1) \\
 &= R_s + jX_s.
 \end{aligned}$$

From which one obtains

$$R_s = r_2 + \frac{r_1 R_p X_p^2 (r_1 + R_p)}{r_1^2 R_p^2 + X_p^2 (r_1 + R_p)^2} \quad (B2)$$

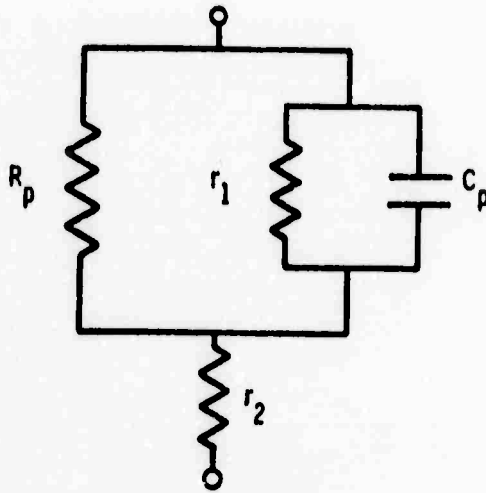


Figure B1. Electrical Model That Produces a Circular Arc Plot

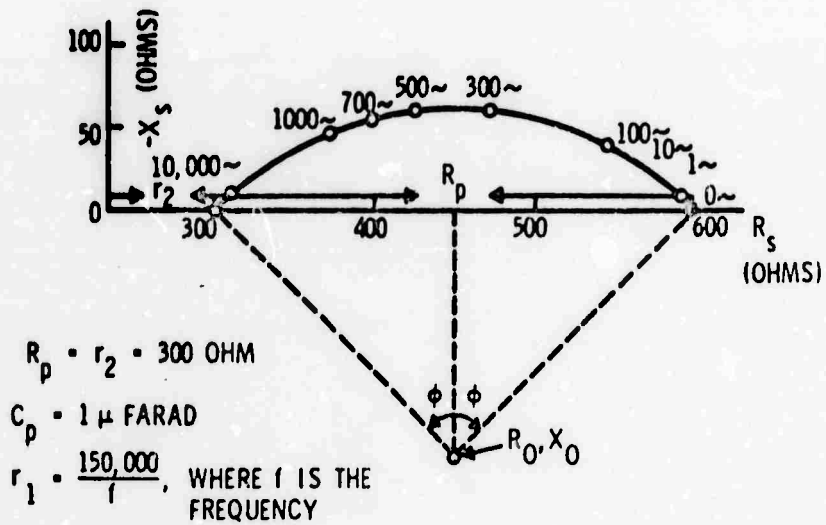


Figure B2. Circular Arc Plot Between Equivalent  $X_s$  and  $R_s$  of the Model

and

$$X_s = \frac{r_1^2 R_p^2 X_p}{r_1^2 R_p^2 + X_p^2 (r_1 + R_p)^2} \quad (B3)$$

Taking the following representative values for the electrical parameters,

$$R_p = r_2 = 300 \text{ ohm}$$

$$C_p = 1 \text{ microfarad}$$

$g = 150,000 \text{ ohm per second}$ , such that  $r_1 = \frac{g}{f} = 300 \text{ ohm}$  at a frequency of 500 Hz, one is able to calculate values for  $R_s$  and  $X_s$  at various frequencies. These calculations are given in Table B1.

Table B1. Equivalent Series Resistance and Reactance for Electrical Model of Figure B1

f Hz	$r_1$ ohm	$X_p$ ohm	$R_s$ ohm	$X_s$ ohm
1	150,000	159,236	599	0.6
10	15,000	15,924	594	5.4
100	1,500	1,592	544	38.3
300	500	531	467	58.9
500	300	318	423	57.8
700	214	227	396	52.8
1,000	150	159	372	45.1
10,000	15	16	308	7.1

The plot of  $X_s$  against  $R_s$  as shown in Figure B2 is found to describe a circular-arc with a depressed center and whose boundary values satisfy the limiting values required by the electrical models of the circuit in Figure B1. Thus, at infinite frequency, both  $r_1$  and  $X_p$  become zero, and the total impedance of the network equals  $r_2$ , i.e., 300 ohm. The first intersection point of the circular-arc with the  $R_s$  axis is also found to be 300 ohm. At zero frequency, the limiting impedance of the network becomes  $(R_p + r_2) = 600$  ohm.

It appears, therefore, that the electrical model of Figure B1 gives a realistic analog to a system displaying a circular-arc plot in the Argand diagram. The limits of the rock impedance at zero frequency would be given by  $(r_2 + R_p)$  and, at infinite frequency, by  $r_2$ . A direct estimation of  $r_2$  and  $R_p$  is thus possible by extrapolating the circular-arc to intersect the real axis. The unusual resistor in this model is  $r_1 = \frac{g}{f}$ , where  $g$  is a constant given by

$$g = \frac{1}{2\pi K C_p} \quad (B4)$$

where  $K$  is a constant related to the phase-angle, and  $C_p$  is the frequency independent rock capacitance which can be taken as a constant.

The rock phase-angle,  $\phi$ , would only be dependent on the values of  $C_p$  and  $r_1$  and, since these two components are in parallel, then

$$\begin{aligned} \phi &= \tan^{-1} \left( \frac{r_1}{X_p} \right) = \tan^{-1} \left[ \frac{1}{K\omega C_p} / \frac{1}{\omega C_p} \right] \\ &= \tan^{-1} \left( \frac{1}{K} \right) \end{aligned} \quad (B5)$$

and, hence,

$$K = \cotan \phi, \text{ or } \phi = \cotan^{-1} K. \quad (\text{B6})$$

The angle,  $\phi$ , would also be identical with the experimentally measured phase-angle between the vertical through the semicircular-arc center and the line joining it to either of its intercepts with the real axis. Thus, experimentally determining the rock phase-angle,  $\phi$ , in each individual case would enable a determination of the constant  $K$  required to calculate  $r_1$ .

To calculate the turnover-frequency, one can make use of the fact that it is the characteristic frequency which maximizes  $X_s$ . Upon differentiating Equation (B3) for  $X_s$  with respect to  $\omega$ , one can easily derive that the turnover angular frequency is given by

$$\omega_{\max} = \frac{1}{R_p C_p \sqrt{1 + K^2}} \quad (\text{B7})$$